catalysts

Review

The Construction and Photocatalytic Application of Covalent Triazine Framework (CTF)-Based Composites: A Brief Review

Yuchen Wei, Quanmei Zhou, Xinglin Wang, Yifan Liao, Jiayi Meng, Yamei Huang, Linlin Gao and Weilin Dai *

State Key Laboratory of Porous Materials for Separation and Conversion, Shanghai Key Laboratory of Molecular Catalysis and Innovative Materials, Department of Chemistry, Fudan University, Shanghai 200438, China; 24110220083@m.fudan.edu.cn (Y.W.); 24110220121@m.fudan.edu.cn (Q.Z.); 21110220106@m.fudan.edu.cn (X.W.); 23110220051@m.fudan.edu.cn (Y.L.); 23110220061@m.fudan.edu.cn (J.M.); 22110220028@m.fudan.edu.cn (Y.H.); 22110220020@m.fudan.edu.cn (L.G.)

* Correspondence: wldai@fudan.edu.cn; Tel.: +86-21-31249122

Abstract: Covalent triazine frameworks (CTFs) are a class of porous organic semiconductors containing a large number of triazine units, which gives them many properties suitable for photocatalysis, such as high porosity, good tunability, and excellent chemical stability. However, it is difficult to achieve high activity, stability, and selectivity at the same time using a single CTF in a specific catalytic reaction. Therefore, it is necessary to find ways to combine CTFs with other materials to improve their photocatalysis activity. From this perspective, some construction methods and the latest progress of CTF-based composites are presented, and their applications in the field of photocatalysis are introduced. Finally, the future of CTF materials in catalytic applications is proposed, which provides some insights into the research and exploration of CTF-based composites.

Keywords: covalent triazine frameworks; photocatalysis; composite design; photocatalytic applications

Academic Editor: Roberto Fiorenza

Received: 28 April 2025
Revised: 30 May 2025
Accepted: 3 June 2025
Published: 5 June 2025

Citation: Wei, Y.; Zhou, Q.; Wang, X.; Liao, Y.; Meng, J.; Huang, Y.; Gao, L.; Dai, W. The Construction and Photocatalytic Application of Covalent Triazine Framework (CTF)-Based Composites: A Brief Review. *Catalysts* **2025**, *15*, 562. https://doi.org/10.3390/catal15060562

1. Introduction

The excessive reliance on fossil fuels has become a major driver of global environmental and climate change, leading to a sharp increase in greenhouse gas emissions, a rise in global temperatures, frequent extreme weather events, and damage to ecosystems. Over-reliance on fossil fuels not only exacerbates atmospheric pollution and the greenhouse effect but also poses a potential risk of energy depletion, threatening energy security and sustainable development [1]. In this context, the application of photocatalytic technology is of significant importance. By utilizing photocatalytic reactions to convert inexhaustible solar energy into chemical energy, it not only helps avoid an energy crisis but also reduces carbon emissions, making it a highly promising approach.

Since Fujishima and Honda discovered that TiO_2 could serve as a photocatalyst for water splitting [2], numerous researchers have dedicated efforts to exploring semiconductor photocatalysts. Various effective photocatalysts have been discovered, including ZnO [3], CdS [4], $BiVO_4$ [5], C_3N_4 [6], COF [7], MOF [8], and others. In recent years, novel materials known as covalent triazine frameworks (CTFs) have gradually gained attention.

As porous organic polymers containing abundant triazine structures, CTF materials possess a large specific surface area, rich nitrogen sites, and π-conjugated structures [9]. These characteristics enable CTF materials to have advantages in both the thermodynamics and kinetics of photocatalytic reactions. However, pure CTF materials still face issues such as fast charge carrier recombination and low visible light utilization efficiency [10]. Therefore, the combination of CTFs with other materials to optimize photocatalytic performance has gradually become a promising research direction.

This brief review primarily focuses on CTF-based composite photocatalytic materials. It introduces several widely studied methods for constructing CTF-based composites, including chemical doping, and the combination of CTFs with non-metals, single atoms, metal oxides, and metal sulfides. This brief review also showcases recent applications of CTF-based composite materials in several major photocatalytic reactions, including photocatalytic hydrogen evolution, photocatalytic H_2O_2 production, photocatalytic CO_2 reduction, and other photocatalytic processes. Finally, the future research directions of CTF-based composite materials in the field of photocatalysis are discussed, with the hope of providing insights for researchers in this field.

2. Composite Design

2.1. Structure and Synthesis of CTFs

In 2008, Thomas et al. [11] used a series of aromatic nitrile monomers to react with molten zinc chloride under high-temperature conditions, preparing a series of materials containing triazine units. These materials exhibit large specific surface areas and porosities, demonstrating excellent gas adsorption properties and stability. These represent the earliest reported CTF materials. The structure of CTF materials can be summarized as follows: a large number of triazine units, which serve as linking groups, connect functionalized monomers to form an ordered conjugated structure (Figure 1). By altering the raw materials and synthesis methods, CTF materials containing different monomers can be prepared. For example, Thomas et al. synthesized CTF-1 [11] and CTF-0 [12] using 1,4-dicyanobenzene and 1,3,5-tricyanobenzene as monomers, respectively. The flexibility and adjustability of the monomers ultimately lead to the CTF materials exhibiting a rich variety of structures, different band gaps, and light-responsive properties, highlighting their extraordinary potential in photocatalysis.

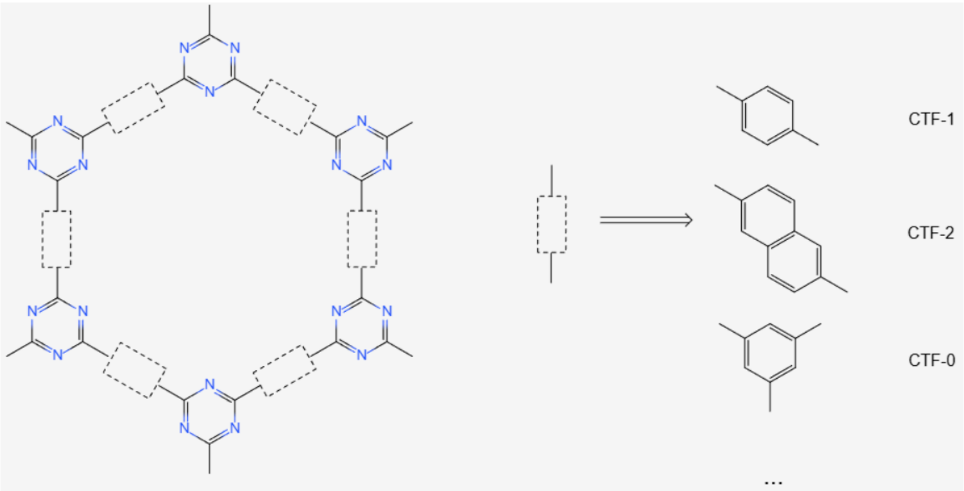

Figure 1. Schematic diagram of the structure of some CTF materials.

Several methods for the synthesis of CTFs have been developed. For instance, the ionothermal polymerization method initially used by Thomas et al. [11] involves the use of molten $ZnCl_2$ as a solvent and catalyst at 400 °C, allowing for the trimerization of 1,4-dicyanobenzene to yield black CTF-1 powder. The disappearance of the cyano group peak at 2218 cm^{-1} and the significant triazine group signal at 1352 cm^{-1} in the infrared spectrum confirmed the successful synthesis of CTFs. Baek et al. [13] innovatively proposed the use of P_2O_5 as a catalyst for the polymerization of terephthalamide to form pCTF-1. pCTF-1 synthesized using this phosphorus-based catalytic method exhibits a larger specific surface area than CTF-1 obtained via ionothermal polymerization; however, the process still requires high temperatures. Additionally, the superacid catalytic method proposed by Cooper et al. [14] is an effective approach for synthesizing CTFs. The team synthesized various CTF materials under both room-temperature and microwave-assisted conditions using trifluoromethanesulfonic acid as the catalyst, naming the materials P1-P6 and P1M-P6M. It was ultimately discovered that the materials synthesized by this method exhibited color changes; for example, P6M was light yellow, which is distinct from the black CTF obtained via traditional $ZnCl_2$ ionothermal polymerization, and demonstrated excellent light-responsive properties. Another synthesis method based on amidine–aldehyde condensation was first proposed by Tan et al. [15]. Using dimethyl sulfoxide as a solvent and Cs_2CO_3 as a base, a series of CTF materials (CTF-HUST-1~4) were synthesized at 120 °C. This method offers milder reaction conditions, avoiding the use of high temperatures and superacid, but the multi-step process presents challenges in terms of synthesis cost and efficiency. In addition to the synthesis of triazine units followed by polymerization into CTFs, CTF materials can also be synthesized by directly using monomers containing triazine units. For example, the Yamamoto coupling reaction and Suzuki coupling reaction have been applied in CTF synthesis [16,17].

Many studies on methods for the synthesis of CTFs have been conducted, and numerous reviews have discussed this research direction. This brief review primarily focuses on CTF-based composite materials, so further elaboration on this topic will not be provided.

2.2. Chemical Doping

To improve the light absorption and charge separation properties of CTFs, it is essential to modify factors such as the electronic band structure, Fermi level, and carrier density. A common and effective method is chemical doping [18,19]. Research has demonstrated that introducing elements like halogens (F, Cl, Br) [20,21], N [22,23], P [24], and S [25] via doping can notably influence the photocatalytic performance of a CTF by altering its electronic configuration. For instance, Cheng et al. [20] synthesized CTF-1 using trifluoromethanesulfonic acid as a catalyst and subsequently mixed it with ammonium halides for thermal treatment to prepare CTF materials doped with different halogen atoms (CTFF, CTFCl, CTFBr). They observed that all three doped materials exhibited narrower band gaps and enhanced charge separation capabilities, ultimately demonstrating superior activity in the photocatalytic hydrogen evolution reaction. Among them, the hydrogen production activity of CTFCl was increased most significantly, and the hydrogen evolution rate was 7.1 times higher than that of undoped materials. The variations in performance due to different doping elements might be linked to their electronegativity and atomic size. Compared to the other two elements (F and Br), chlorine's more suitable electronegativity and atomic size may provide important insights into this behavior (C: 2.55, 0.67 Å; N: 3.04, 0.56 Å; F: 3.98, 0.42 Å; Cl: 3.16, 0.79 Å; Br: 2.96, 0.94 Å). Moreover, Cheng et al. [24] investigated the effects of phosphorus doping on a CTF. In this case, the composite material was prepared by mixing a CTF with red phosphorus and subjecting it to simple thermal treatment at 250 °C for one hour. The phosphorus-doped CTF material demonstrated superior photocatalytic hydrogen absorption due to enhanced visible light absorption and photocatalytic electron reduction capabilities, improving the separation and transfer of photogenerated carriers.

A nitrogen-doped CTF (NCTF-1) [22] was synthesized by hydrothermally treating CTF-1 with hydrazine hydrate. Compared to unmodified CTFs, NCTF-1 has a higher nitrogen content. This provides more basic sites for the material, improving its CO_2 adsorption ability. Consequently, it achieved an activity of 11.48 $\mu mol \cdot g^{-1} \cdot h^{-1}$ in photocatalytic

CO_2 reduction to CH_4, which was nine times higher than that of bare CTF-1. In another study, Han et al. [23] created a different nitrogen-doped CTF (T3N-CTF) by the Schiff base reaction. The additional three pyridine nitrogen atoms around the triazine unit provide more active sites for hydrogen production, reduce the recombination of electrons and holes, and improve charge transport at the catalyst surface.

S-doped CTF [25] materials also exhibit enhanced photocatalytic performance and stability. When compared to the original CTF-T1, the composite material showed a faster separation and transfer of photogenerated electron–hole pairs (Figure 2a–d). Theoretical models [26] suggest that this improvement is due to sulfur impurity atoms, which introduce asymmetric impurity energy levels near the Fermi level, promoting electron spin polarization and creating an internal electric field (IEF). This aids the migration of photogenerated carriers in a specific direction, preventing recombination (Figure 2e,f).

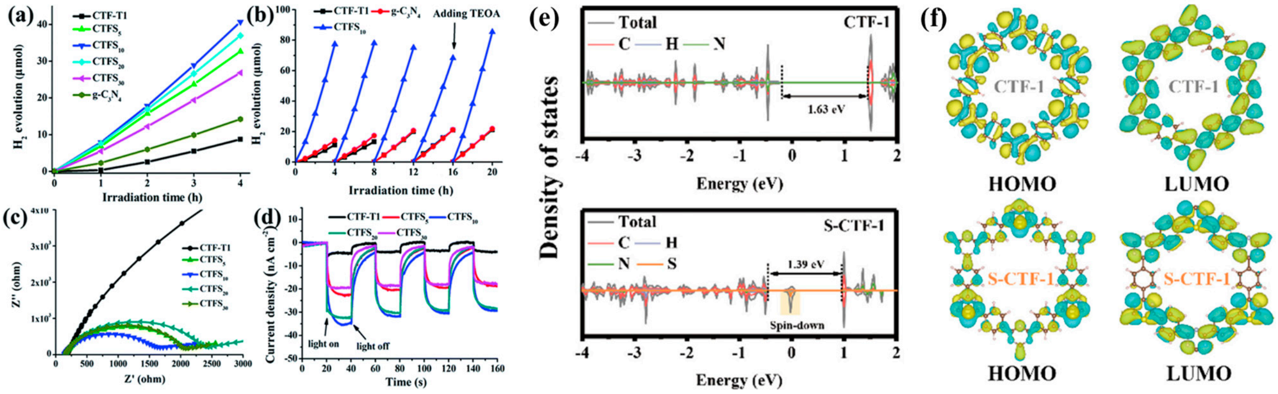

Figure 2. (**a**) A comparison of the photocatalytic hydrogen generation performance of various samples (CTF-T1, $CTFS_X$, and $g-C_3N_4$) over a period of four hours. (**b**) Stability assessment of photocatalytic hydrogen production for five consecutive cycles with different samples. (**c**) Nyquist plots from electrochemical impedance spectroscopy (EIS). (**d**) Photocurrent response curves for both CTF-T1 and $CTFS_X$. Reproduced with the permission of ref. [25]. Copyright 2016, Royal Society of Chemistry. (**e**) The density of states and (**f**) HOMO and LUMO surface plots for a pure CTF and S-doped CTF. Reproduced with the permission of ref. [26]. Copyright 2022, American Chemical Society.

Doping with other elements in a CTF that is an organic semiconductor is more challenging than in inorganic semiconductors because doping typically disrupts its original covalent bonds. This implies that the conjugated structure of the CTF is disrupted, leading to a decrease in crystallinity. Moreover, achieving the precise insertion of dopants at specific positions within CTF materials is also highly challenging. Compared to inorganic semiconductors, these difficulties make the doping process in CTF materials more complex and harder to control.

2.3. Composite with Non-Metallic Materials

Non-metallic materials such as carbon nitride (C_3N_4) and black phosphorus (BP) nanosheets, with their remarkable optical characteristics and electrical conductivity, have been widely explored to form heterojunctions with CTFs, which improves the visible light absorption and charge transfer capabilities of CTF-based photocatalysts [27,28]. For instance, He et al. [27] were the first to combine a CTF with $g-C_3N_4$ to create a 2D/2D heterostructure aimed at photocatalytic CO_2 reduction. By using $Co(bpy)_3Cl_2$ as a co-catalyst, the composite material achieved 99% efficiency in the selective photocatalytic reduction of CO_2 to CO. Regarding its stability, the CO production rate remained largely unaffected after three cycles over 30 h. Zhang et al. [28] proposed a method for synthesizing the CTF/BP composite, where a CTF was applied onto BP nanosheets via sonication.

Under light exposure, the photogenerated electrons efficiently transferred from the CTF to the BP surface through the P-C bond, and the accumulated electrons protected the BP nanosheets from surface oxidation. This composite exhibited excellent photocatalytic hydrogen production, reaching an activity of 17.1 mmol·g^{-1}·h^{-1} when formaldehyde was used as a sacrificial agent.

As a carbon-based material, carbon quantum dots (CQDs) not only demonstrate high electrical conductivity but also show outstanding biocompatibility and photoluminescence (PL) due to their size being under 10 nm [29]. Yang et al. [30] proposed loading CQDs onto a CTF to boost electron transfer efficiency and photocatalytic performance (Figure 3a). The results indicated that CQDs in the composite acted as electron transfer mediators, significantly enhancing conductivity, and exhibited photocatalytic H_2O_2 production of 1036 μmol·g^{-1}·h^{-1}, which was 4.6 times greater than the activity of a pure CTF (Figure 3b,c).

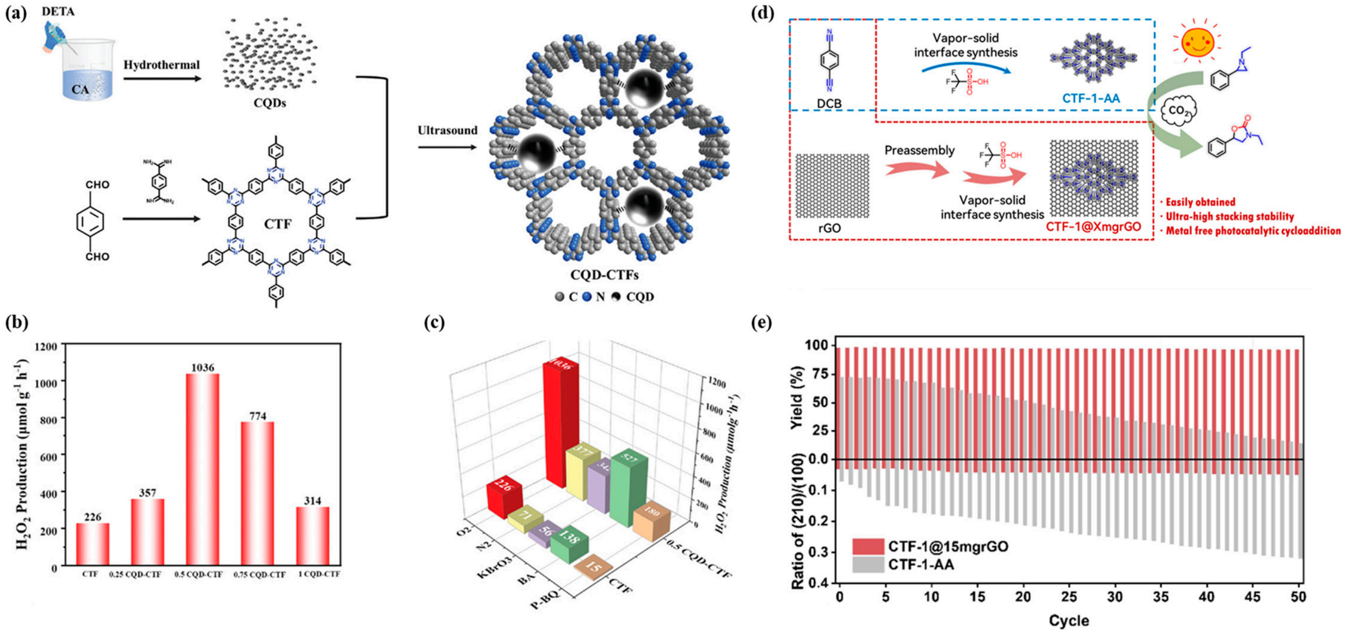

Figure 3. (**a**) Diagram illustrating the synthetic pathway of CQD-CTFs. (**b**) Photocatalytic H_2O_2 generation efficiency of CQD-CTFs. (**c**) Mechanistic experiments for capturing intermediates during photocatalytic H_2O_2 production. Reproduced with the permission of ref. [30]. Copyright 2024, Wiley-VCH. (**d**) Diagram outlining the synthesis steps of CTF-1-AA and CTF-1@XmgrGO. (**e**) Experimental results showing the performance after 50 cycles of CTF-1@15mgrGO and CTF-1-AA. Reproduced with the permission of ref. [31]. Copyright 2025, Elsevier.

In contrast, Chen et al. [31] developed the AA-stacked CTF-1@rGO composite, which exhibits exceptional solvent stability, using a two-step synthesis approach (first, monomers are pre-assembled on the rGO surface, followed by gas–solid interface catalytic synthesis) (Figure 3d). The addition of rGO improved the crystallinity of the composite material and enhanced its structural stability during stacking. The CTF-1@15mgrGO catalyst demonstrated consistent photocatalytic activity over 50 cycles, indicating superior durability when compared to the CTF-1-AA alone (Figure 3e).

2.4. Single Atoms

Single-atom catalysts (SACs) offer numerous active sites and achieve nearly perfect atomic utilization (close to 100%). Additionally, they can be immobilized on photocatalyst surfaces, facilitating the high-efficiency dissociation of photogenerated carriers, which makes them a key area of study in photocatalysis [32–34]. However, SACs have high surface free energy, causing them to aggregate, which reduces their catalytic performance.

To counteract this challenge, nitrogen-enriched CTFs have emerged as promising materials to improve the dispersion and stability of SACs. In recent years, various single atoms, such as Pt [35], Fe [36], Ni [37,38], Pd [39], Ir [40], Cu [41], Co [42], Ti [43], and others, have been successfully anchored onto CTFs for various photocatalytic tasks.

Zhu et al. [44] pioneered the synthesis of Py-CTF, a material rich in pyridine nitrogen sites, using a ligand engineering approach. Subsequently, under the combined influence of two nitrogen species and a confined channel structure, Co atoms were anchored as single atoms onto Py-CTF nanosheets (Co_{SA}/Py-CTF). This composite showed remarkable photocatalytic activity for H_2O_2 production (2898.3 $\mu mol \cdot g^{-1} \cdot h^{-1}$). Furthermore, the apparent quantum yield (AQY) reached its maximum value of 13.2% at 420 nm (Figure 4a,b). Significantly, in situ XAFS experiments tracked the dynamic changes in the coordination structure of Co sites during photocatalysis. Upon exposure to light and O_2 adsorption, the Co-N_3 sites in Co_{SA}/Py-CTF were altered, with the Co-N bonds stretching and the coordination number decreasing. As a result, Co single atoms were released and formed transient atomic pairs with neighboring Co atoms, promoting the conversion of the O_2 adsorption configuration from the Pauling type to the Yeager type, thereby triggering a one-step, two-electron oxygen reduction reaction. Following the reaction, the Co atom pairs returned to their original single-atom form, restoring the catalyst (Figure 4c–g).

Meanwhile, Liu et al. [45] modified the synthesis of a triazine-deficient CTF by substituting part of 1,4-dicyanobenzene with 4-cyanopyridine. They subsequently incorporated Ni single atoms, creating a covalent triazine framework (d-CTF-Ni) with both Ni and pyridine N acting as dual active sites (Figure 4h). In this structure, Ni single atoms function as centers for electron capture, aiding the O_2 reduction process, while the pyridine N, owing to its electronic deficiency, serves as hole acceptors to enhance the water oxidation reaction. The combined effect of these two processes greatly boosts the photocatalytic generation of H_2O_2, leading to superior activity of the composite material (Figure 4i–k).

2.5. Compounded with Metal Oxides

TiO_2, a prominent member of the metal oxide group in semiconductor photocatalysis, has attracted significant attention due to its exceptional chemical stability, non-toxic nature, resistance to corrosion, and cost-effectiveness. The semiconductor characteristics of TiO_2 allow it to capture light energy within a particular wavelength range, facilitating the excitation of electrons from the valence band to the conduction band, which in turn drives surface redox reactions. However, photocatalytic processes involving TiO_2 are hindered by several issues, such as its large bandgap, slow charge carrier transfer rate, and limited photocatalytic efficiency. To address these challenges, researchers have explored combining TiO_2 with covalent triazine frameworks as a support material, resulting in composites that have been successfully used in a variety of photocatalytic applications [46–48]. For instance, a bifunctional heterojunction was created by incorporating TiO_2 particles onto CTF sheets using a simple impregnation method, with the goal of improving both the adsorption and photocatalytic degradation of ciprofloxacin [49]. In contrast to the broad bandgap (3.20 eV) of pure TiO_2, the bandgap of this composite material was significantly reduced to 2.86 eV, leading to enhanced photocatalytic performance. The CT-2 composite (with a CTF/TiO_2 mass ratio of 1:2) achieved a 77.5% photodegradation rate for ciprofloxacin within 120 min, while the CT-2/H_2O_2 system boosted the rate to 90.7% in just 40 min (Figure 5a,b). An S-scheme heterojunction was formed between a CTF and TiO_2, based on their respective energy band structures. Under visible light exposure, electrons and holes accumulated on the CTF and TiO_2, respectively, causing band bending, which, in combination with H_2O_2, accelerated ciprofloxacin degradation (Figure 5c). In another investigation, an AA-stacked CTF-TiO_2 heterojunction (CTF-AA/TiO_2) was fabricated for photocatalytic CO_2 reduction [50]. Compared to AB-stacked materials, the CTF-AA/TiO_2 showed a stronger photocurrent response, a faster charge transfer rate at the interface, and more efficient electron–hole separation, ultimately demonstrating superior CO_2 reduction capability.

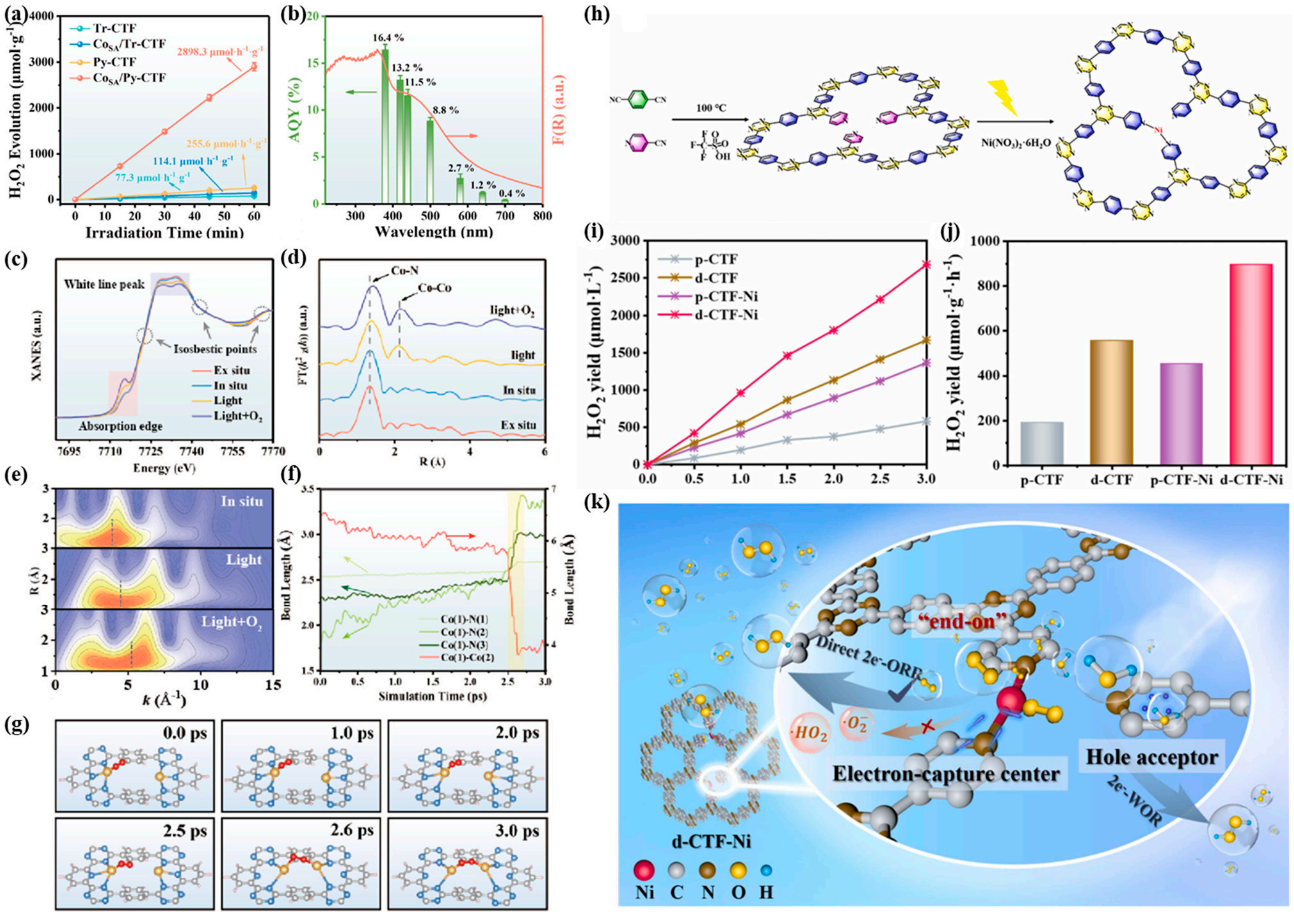

Figure 4. (**a**) A comparison of the catalytic performance of various catalysts (Tr-CTF, Co_{SA}/Tr-CTF, Py-CTF, and Co_{SA}/Py-CTF) in photocatalytically generating hydrogen peroxide in pure water over a 60 min period. (**b**) The correlation between the apparent quantum yield of Co_{SA}/Py-CTF for hydrogen peroxide production and the wavelength of incoming light. (**c**) Co K-edge XANES spectra of Co_{SA}/Py-CTF recorded under ex situ, in situ, and illuminated conditions and under conditions of illumination with O_2 supply. (**d**) Fourier-transformed EXAFS spectra and (**e**) corresponding wavelet transform EXAFS spectra of Co_{SA}/Py-CTF under various conditions. (**f**) Simulation of Co-N bond length variations during the photocatalytic reaction using ab initio molecular dynamics. (**g**) Dynamic changes in the Co_{SA}/Py-CTF structure illustrated by key snapshots from ab initio molecular dynamics simulations. Reproduced with the permission of ref. [44]. Copyright 2024, American Chemical Society. (**h**) The synthetic approach and structure of CTF-Ni composites. (**i**) Under visible light irradiation, the H_2O_2 production time profiles for different catalysts. (**j**) H_2O_2 yield of each catalyst after 3 h of testing. (**k**) Schematic representation of CTF-Ni composites for photocatalytic H_2O_2 production. Reproduced with the permission of ref. [45]. Copyright 2023, Elsevier.

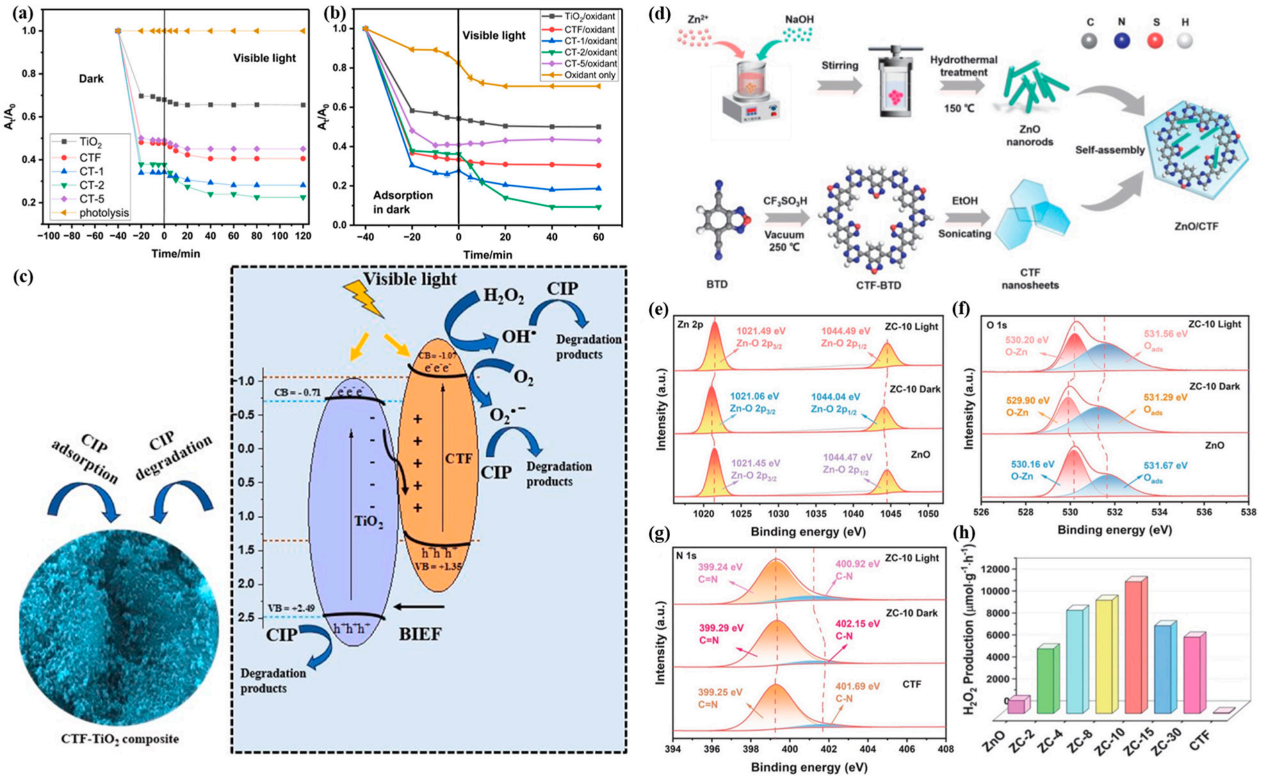

Figure 5. (**a**) Adsorption and photocatalytic degradation at a temperature of 25 °C. (**b**) Adsorption and photocatalytic oxidation (conditions identical to (**a**), but with the addition of 10 mM H_2O_2 as an oxidant). (**c**) Mechanism of ciprofloxacin degradation via the composite system under adsorption and photocatalytic conditions. Reproduced with the permission of ref. [49]. Copyright 2024, Elsevier. (**d**) Synthesis procedure for ZnO/CTF samples. (**e**) Zn 2p XPS spectra of ZnO and ZC-10. (**f**) O 1s XPS spectra of ZnO and ZC-10. (**g**) N 1s XPS spectra of the CTF and ZC-10. (**h**) Activity comparison of various samples (ZnO, CTF, and ZC-x) in H_2O_2 production. Reproduced with the permission of ref. [51]. Copyright 2025, Elsevier.

ZnO is another well-known metal oxide. Despite its inherently large bandgap, which restricts its activation to ultraviolet light, it not only acts as an oxidizing photocatalyst (OP) but also serves as an excellent electron-donating photocatalyst [52,53]. Building on this, Xia et al. [51] endeavored to create an S-scheme heterojunction made of ZnO and a CTF to enhance photocatalytic H_2O_2 production (Figure 5d). Their study showed that in situ XPS measurements indicated a reversal of the peak shift direction before and after exposure to light. Under dark conditions, ZnO absorbs electrons, but when exposed to light, it releases them, providing solid proof of the formation of the S-scheme heterojunction (Figure 5e–g). The resulting composite demonstrated remarkable photocatalytic H_2O_2 generation, achieving 12,000 $\mu mol \cdot g^{-1} \cdot h^{-1}$, a performance 10.3 times superior to that of ZnO material and 164 times greater than that of the CTF (Figure 5h).

2.6. Compounded with Metal Sulfides

A widely studied composite material based on a CTF includes its combination with metal sulfides [54–56]. By incorporating MoS_2 quantum dots into CTFs, the photocatalytic hydrogen production rate can be enhanced, reaching a value up to 8 times higher than that of the unmodified material [57]. However, increasing the MoS_2 concentration beyond a certain point leads to the obstruction of active sites, thus reducing photocatalytic efficiency. Huang et al. [58] employed a straightforward photoreduction technique to integrate CdS quantum dots with CTF-1. They observed that the favorable band alignment between the two materials facilitated the formation of a type-II heterojunction, which significantly improved the separation and migration of photogenerated charge carriers. Under visible light exposure, the CdS/CTF-1 composite showed a photocatalytic hydrogen evolution rate that was 55 times greater than that of the bare CTF material. Zhang et al. [59] further developed a photocatalyst with a core–shell structure, where CdS nanospheres formed the core, enveloped by a CTF layer (Figure 6a). The electron transfer mechanism facilitated rapid recombination of conduction band electrons from the CTF component and valence band holes from the CdS, generating carriers with superior redox potential and resulting in the formation of an S-scheme heterojunction. Additionally, the porous CTF shell significantly enhanced the composite's CO_2 adsorption capacity. As a result, the photocatalytic CO_2 reduction reaction achieved an $R_{electron}$ value of 389.22 $\mu mol \cdot g^{-1} \cdot h^{-1}$, which was 2.57 times and 4.74 times greater than those of the individual CdS and CTF components, respectively (Figure 6b–e).

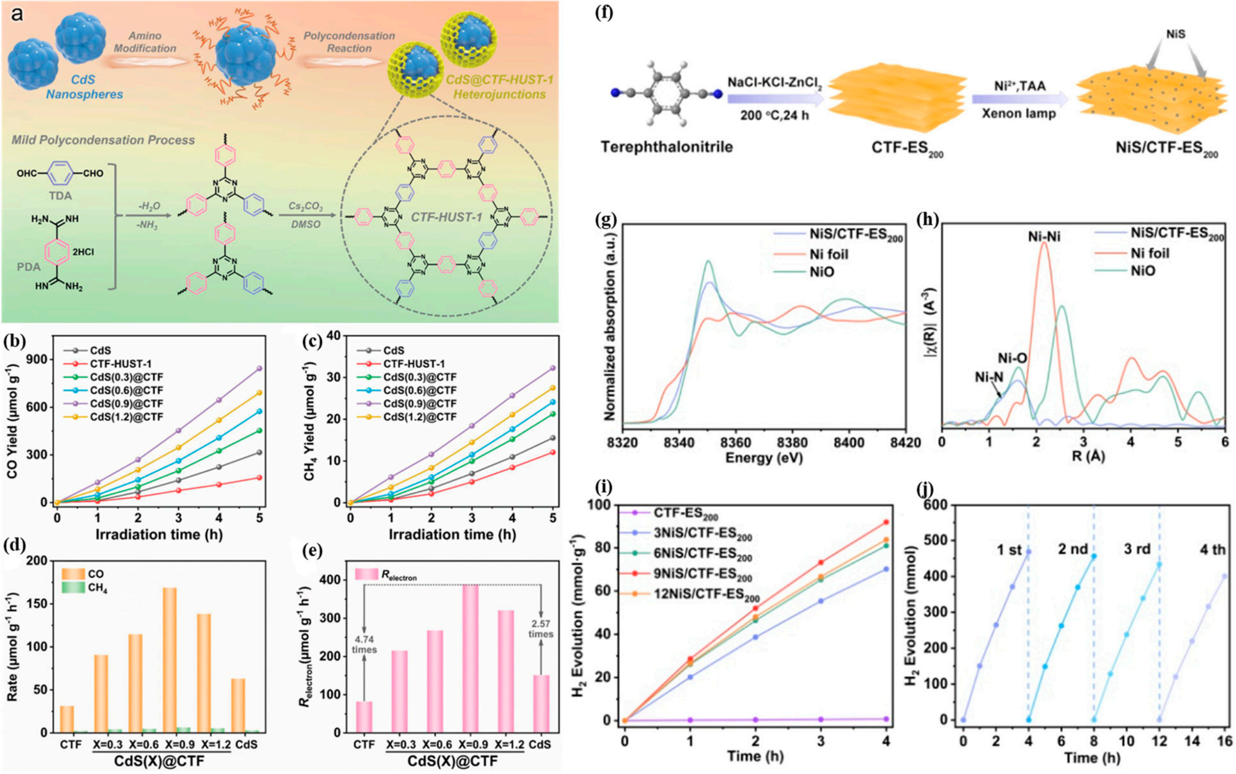

Figure 6. (**a**) Diagram illustrating the synthesis process of CdS@CTF-HUST-1 core–shell heterojunction photocatalysts. (**b**) CO production rates and (**c**) CH_4 production rates for different photocatalysts (CdS, CTF-HUST-1, and CdS(x)@CTF) during a 5 h photocatalytic CO_2 reduction reaction. (**d**) CO and CH_4 generation rates for various samples after the 5 h photocatalytic CO_2 reduction reaction. (**e**) Comparative analysis of $R_{electron}$ values across different samples. Reproduced with the permission of ref. [59]. Copyright 2023, Wiley-VCH. (**f**) Diagram showing the synthesis of NiS/CTF-ES_{200}. (**g**) Ni K-edge XANES spectra. (**h**) Fourier-transformed EXAFS spectra of the Ni K-edge for different samples (NiS/CTF-ES_{200}, Ni foil and NiO). (**i**) Comparison of photocatalytic hydrogen production efficiency for different samples over a four-hour period. (**j**) Photocatalytic hydrogen production performance of 9NiS/CTF-ES_{200} across four continuous cycles. Reproduced with the permission of ref. [60]. Copyright 2024, Elsevier.

Zhou et al. [60] investigated the use of small NiS nanoparticles and successfully developed a photocatalyst featuring a p-n heterojunction (NiS/CTF-ES_{200}) via a simple and environmentally friendly photodeposition technique. This method involved embedding NiS, a material with a narrow band gap and high electrical conductivity, onto CTF-ES_{200} (Figure 6f). The creation of the p-n heterojunction triggered the buildup of photo-generated electrons in the conduction band of CTF-ES_{200}, which in turn preserved a strong reduction potential for the hydrogen evolution reaction and markedly improved the efficiency of photoelectron usage. Furthermore, EXAFS analysis confirmed the formation of Ni-N bonds within the composite, which promoted more efficient transmission of interfacial charge carriers (Figure 6g,h). These synergistic effects resulted in the NiS/CTF-ES_{200} composite demonstrating remarkable photocatalytic hydrogen production activity, with a rate of 22.98 $mmol \cdot g^{-1} \cdot h^{-1}$, greatly surpassing that of the pure CTF material (Figure 6i,j).

3. Photocatalytic Application of CTF-Based Composites

CTFs have emerged as prominent materials in semiconductor photocatalysis due to their distinctive and stable structure, high nitrogen content, and adaptable functional groups. In recent times, CTF-based composites have found extensive use in various photocatalytic applications. The purpose of this section is to review the advancements in the development and utilization of CTF-based composites in several photocatalytic fields, including hydrogen production, oxygen evolution, H_2O_2 synthesis, CO_2 reduction, and pollutant remediation.

3.1. Photocatalytic Hydrogen Evolution

Hydrogen is acknowledged as one of the most high-potential clean and sustainable energy solutions, significantly contributing to alleviating energy crises and environmental pollution. Under the action of a catalyst, utilizing solar energy to complete the reduction reaction of hydrogen ions to hydrogen gas in water is considered a promising method for hydrogen production. C_3N_4 has been extensively studied as a photocatalyst for hydrogen generation, and CTF materials, with their abundant triazine units, share similar properties to C_3N_4 [61,62]. A substantial body of research has explored the use of CTF-based composites for photocatalytic hydrogen production [63–69]. Table 1 shows the comparison of different CTF-based composites in photocatalytic hydrogen evolution reactions.

Table 1. Performance comparison of CTF-based composites for photocatalytic hydrogen production.

Photocatalyst	Cocatalyst	Sacrificial Reagent	Light Source	HER ($\mu mol\ g^{-1} \cdot h^{-1}$)	AQE (%)	Ref.
TAPT-COF-CQDs	Pt (3 wt%)	TEOA	300 W Xe lamp ($\lambda > 420$ nm)	69,570	9.5 (440 nm)	[63]
PtSA@S-TFPT	/	TEOA	300 W Xe lamp ($\lambda > 420$ nm)	11,400	4.65 (420 nm)	[64]
CTF-Cu_2O@NC	Pt (3 wt%)	TEOA + MeOH	300 W Xe lamp ($\lambda > 420$ nm)	15,645	1.67 (420 nm)	[65]
Co_1-PCTF	/	TEOA	300 W Xe lamp ($\lambda > 420$ nm)	2562.4	10.22 (365 nm)	[67]
TMT-BO-COF	Pt (5 wt%)	AA	300 W Xe lamp	23,700	0.11 (420 nm)	[68]
Pt@CTF-Py-1	/	TEA	AM 1.5 G	14,960	4.51 (420 nm)	[69]

For example, Chen et al. [64] developed a photocatalyst called PtSA@S-TFPT, incorporating low-valent platinum single atoms into a sulfur-containing COF. During synthesis, Pt was reduced to its low-valent state using methanol, forming four stable asymmetric coordination bonds with sulfur/oxygen sites, which prevented particle aggregation. Under the illumination of a 300 W Xenon lamp, with triethanolamine as a sacrificial agent, PtSA@S-TFPT demonstrated excellent stability during three 3 h cyclic hydrogen evolution reaction tests, achieving an average hydrogen production rate of 11.44 $mmol \cdot g^{-1} \cdot h^{-1}$. At 420 nm, the material exhibited a maximum apparent quantum yield of 4.65%. Electrochemical analysis showed that PtSA@S-TFPT exhibited a higher photocurrent and lower impedance and reduced photoluminescence intensity, suggesting that the presence of Pt single atoms significantly enhanced the migration and separation of photo-generated carriers, boosting catalytic activity.

Pyridine can be considered a structure where one carbon atom in the benzene ring is replaced by nitrogen. Due to the higher electronegativity of nitrogen, electrons accumulate at the nitrogen atom. This gives pyridine a strong coordination ability, making it an effective carrier for metal atoms to anchor. Based on this idea, Yao et al. [67] developed a pyridine-enriched CTF modified with Co single atoms (Co_1-PCTF), which served as an efficient catalyst for photocatalytic hydrogen production. For this, 2,6-pyridine dicarbonitrile (2,6-DCPY) was chosen as the monomer for polymerizing PCTF, providing abundant nitrogen sites to anchor Co single atoms (Figure 7a). XAFS analysis was employed to examine the valence state and coordination environment of Co atoms in the Co-CTF composite material. XANES results showed that the Co absorption edge in Co_1-PCTF was positioned higher than that of Co foil, but lower than that of CoO, indicating an oxidation state of 0 to +2 (Figure 7b). EXAFS data revealed that no Co-Co peaks were observed in Co_1-PCTF, but a distinct peak at 1.68 Å was attributed to the Co-N bond. Fitting analysis indicated that Co atoms in the material formed coordination bonds with three surrounding nitrogen atoms (Figure 7c,d). Under visible light, using TEOA as a sacrificial agent for photocatalytic hydrogen evolution, the hydrogen evolution rate of Co_1-PCTF was 2562.4 $\mu mol \cdot g^{-1} \cdot h^{-1}$, several times higher than that of other pure and composite materials (Figure 7e). The material's AQY peaked at 10.22% at 365 nm, displaying significant wavelength dependence (Figure 7f). In terms of stability, the material maintained excellent hydrogen evolution performance after six consecutive 4 h cycles, with only a 4.86% decrease in efficiency (Figure 7g). Furthermore, the authors synthesized a series of transition metal single-atom-modified M_1-PCTFs (Figure 7h). Among them, Co_1-PCTF demonstrated the best photocatalytic hydrogen production rate, attributed to the unsaturated d orbitals of Co, efficient electron capture, and its unique coordination bond with pyridine nitrogen.

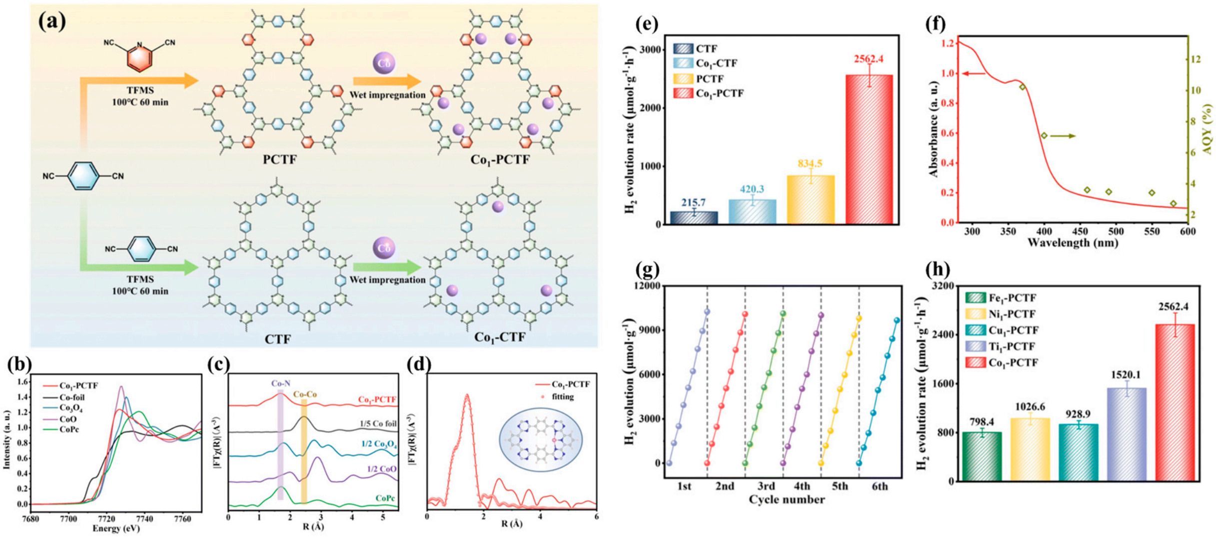

Figure 7. (**a**) Illustration of the Co_1-PCTF photocatalyst synthesis process. (**b**) Co K-edge XANES spectra and (**c**) Fourier-transformed EXAFS spectra for various samples (Co_1-PCTF, Co foil, Co_3O_4, CoO, and CoPc). (**d**) EXAFS fitting curves of Co_1-PCTF. (**e**) Comparison of photocatalytic hydrogen production activity across different samples (CTF, Co_1-CTF, PCTF, and Co_1-PCTF). (**f**) Relationship between Co_1-PCTF's AQY for photocatalytic hydrogen production and incident light wavelength. (**g**) Performance of Co_1-PCTF in photocatalytic hydrogen production over six consecutive cycles. (**h**) Comparison of the activity of PCTF materials loaded with different transition metal single atoms in photocatalytic hydrogen production reactions. Reproduced with the permission of ref. [67]. Copyright 2024, Royal Society of Chemistry.

3.2. Photocatalytic Production of Hydrogen Peroxide

The conventional method for producing hydrogen peroxide (H_2O_2) in industry is the anthraquinone oxidation process. However, this technique often comes with significant risks and generates numerous by-products that negatively impact energy consumption, the environment, and other factors. As an alternative, using light energy to drive redox or water oxidation reactions has gained attention as a promising approach for H_2O_2 production. Given the outstanding performance of CTF materials in photocatalytic hydrogen production, some researchers are now exploring their potential for photocatalytic H_2O_2 production [70–74]. Table 2 shows a comparison of different CTF-based composites in photocatalytic H_2O_2 production reactions.

Table 2. Performance comparison of CTF-based composites for photocatalytic H_2O_2 production.

Photocatalyst	Cocatalyst	Sacrificial Reagent	Light Source	H_2O_2 Yields (μmol $g^{-1}\cdot h^{-1}$)	AQE (%)	Ref.
F-ol-COF	/	HMF	300 W Xe lamp ($\lambda > 420$ nm)	12,558	13.2 (420 nm)	[70]
TAPT-TFPA COFs@Pd IC	/	EtOH	300 W Xe lamp ($\lambda > 400$ nm)	2143	6.5 (400 nm)	[71]
CDs@CTFs CsCl	/	$NaIO_3$	AM 1.5 G	2464	13.0 (500 nm)	[72]
CNT@COF-H	/	IPA	AM 1.5 G	1581	34.0 (500 nm)	[73]
TF_{50}-COF	/	EtOH	300 W Xe lamp ($\lambda > 400$ nm)	1739	5.1 (400 nm)	[74]

Zhang et al. [70] developed CTF materials with varying degrees of F substitution for use in photocatalytic H_2O_2 production and the oxidation of 5-hydroxymethylfurfural (HMF) to create functionalized furans. The introduction of F atoms in the material can form a p-π conjugated structure with the olefin bond, which improves the charge separation. H-ol-CTF, used as a control, was synthesized using 2,4,6-trimethyl-1,3,5-triazine (TMTA) and terephthalaldehyde (TA). The introduction of the F atom was performed by substituting TA with 2,3,5,6-tetrafluoroterephthalaldehyde (TFTA), resulting in F-ol-CTF. The synthesis process involved reacting TA and TFTA in a 1:1 molar ratio with TMTA to create partially fluorinated HF-ol-CTF (Figure 8a). F-ol-CTF exhibited the lowest photoluminescence intensity and the longest charge carrier lifetime among the three materials (Figure 8b,c), demonstrating its superior charge separation and transfer properties. These characteristics contributed to its highest photocatalytic H_2O_2 production activity of 12,558 $\mu mol\cdot g^{-1}\cdot h^{-1}$, surpassing that of HF-ol-COF (9382 $\mu mol\cdot g^{-1}\cdot h^{-1}$) and H-ol-CTF (6373 $\mu mol\cdot g^{-1}\cdot h^{-1}$), along with excellent apparent quantum yield and stability. Furthermore, the conversion rate of HMF to functionalized furan was significantly higher with this material than with H-ol-COF and HF-ol-COF, reaching 95% after 12 h (Figure 8d–g).

In a similar approach, Liu et al. [71] introduced a fluorinated CTF material for H_2O_2 production, which also featured Pd metal clusters (TAPT-TFPA COFs@Pd ICs) embedded within the material's pores (Figure 9a). TEM and HRTEM analysis revealed that the Pd ICs had an average size of 2.4 nm, which closely aligned with the pore dimensions of the CTF material (Figure 9b,c). The photocatalytic H_2O_2 production activity of the material was tested under visible light irradiation, and the results showed that the material with 3% Pd content provided the highest H_2O_2 generation rate (2143 $\mu mol\cdot g^{-1}\cdot h^{-1}$). Compared with unfluorinated materials, the fluorinated CTF had better catalytic activity. Notably, the photocatalytic efficiency of the composite material was maintained for over 100 h, significantly outperforming other reported photocatalysts (Figure 9d–g). The results of the density of states (DOS) calculations explained the role of Pd in photocatalytic reactions. In the fluorinated COF material, the Pd d-band centers were lower than those observed in the non-fluorinated COF material (Figure 9h,i). These lower d-band centers were linked to weaker binding energies between the Pd IC and intermediate oxygen, which facilitated the easier desorption of the products (Figure 9j).

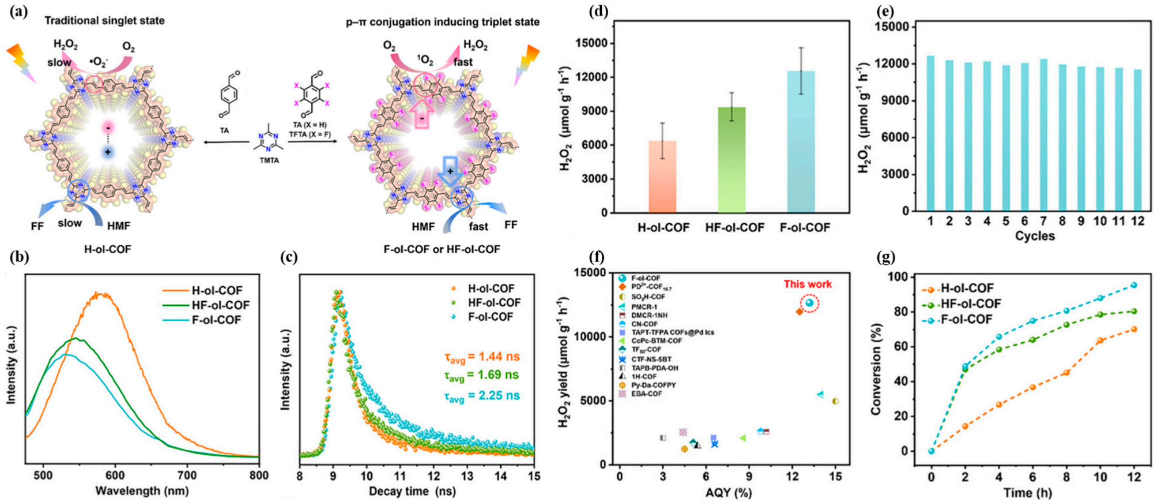

Figure 8. (**a**) Schematic representation of H-ol-COF, HF-ol-COF, and F-ol-COF featuring different charge separation/transfer ability and O_2 activation mechanisms. (**b**) Photoluminescence spectra of H-ol-COF, HF-ol-COF, and F-ol-COF, measured at an excitation wavelength of 455 nm. (**c**) Time-resolved photoluminescence (TRPL) data. (**d**) Comparative photocatalytic H_2O_2 production activity of the three samples. (**e**) Durability of F-ol-COF in photocatalytic H_2O_2 generation (λ > 420 nm). (**f**) Photocatalytic H_2O_2 production activity and apparent quantum yield comparison of F-ol-COF with other COF-based photocatalysts. (**g**) Conversion of HMF across 12 consecutive photocatalysis cycles. Reproduced with the permission of ref. [70]. Copyright 2025, Wiley-VCH.

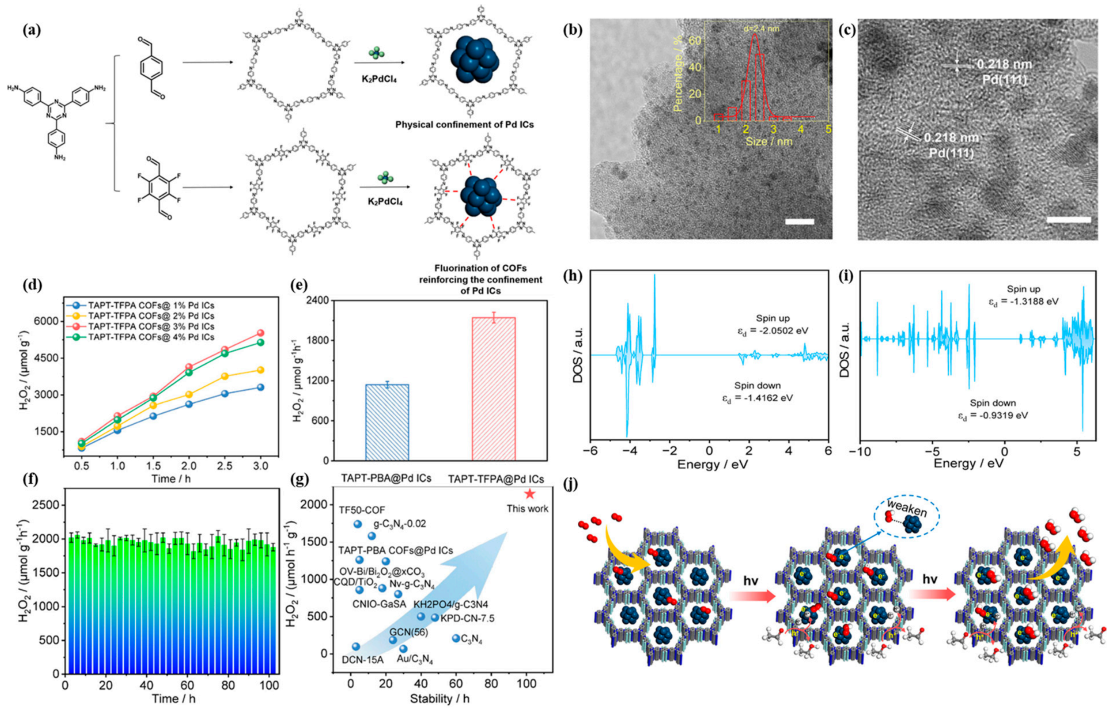

Figure 9. (**a**) Diagram illustrating the fabrication process of the composite materials, where non-fluorinated COFs are used to physically trap Pd ICs, and fluorinated COFs enhance the confinement of Pd ICs. (**b**) TEM and (**c**) HRTEM images of the fluorinated COF-Pd IC composite, with scale bars

of 10 nm and 5 nm, respectively. (**d**) Activity comparison of photocatalysts with varying Pd concentrations in hydrogen peroxide production over a three-hour period. (**e**) Photocatalytic H_2O_2 production rates of the two COF-Pd IC composites. (**f**) Stability of the fluorinated COF-Pd IC composites for long-term photocatalytic H_2O_2 generation. (**g**) Comparative analysis of the performance and durability of the fluorinated COF-Pd IC composites and other photocatalysts in the hydrogen peroxide photocatalysis reaction. (**h**) Calculation of the DOS and Pd d-band center in the fluorinated COF-Pd IC composite. (**i**) Calculation of the DOS and Pd d-band center in the non-fluorinated COF-Pd IC composite. (**j**) Proposed mechanism for photocatalytic hydrogen peroxide production by the fluorinated COF-Pd IC composite. Reproduced with the permission of ref. [71]. Copyright 2023, American Chemical Society.

3.3. Photocatalytic Carbon Dioxide Reduction

Excessive carbon dioxide emissions have emerged as a key contributor to global climate change, exacerbating the greenhouse effect, accelerating global warming, frequent extreme weather events, and ecosystem imbalance, all of which pose serious threats to both human society and the natural environment. Photocatalytic CO_2 reduction presents a promising solution, as it effectively lowers atmospheric CO_2 levels, mitigates the greenhouse effect, and generates alternative fuels, facilitating the shift towards a more sustainable energy system. Covalent triazine frameworks are characterized by a large specific surface area and abundant nitrogen sites, which are advantageous for CO_2 adsorption. However, as organic polymers, CTFs alone often show limited photocatalytic CO_2 reduction efficiency due to their relatively high exciton binding energy [75]. Therefore, researchers have constructed CTF-based composite materials to improve charge transfer and photocatalytic performance [76–85]. Table 3 shows a comparison of different CTF-based composites in photocatalytic CO_2 reduction reactions.

Table 3. Performance comparison of CTF-based composites for photocatalytic CO_2 reduction.

Photocatalyst	Photosensitizer	Sacrificial Reagent	Light Source	CO_2RR Activity	Selectivity (%)	Ref.
CTF-240	/	/	300 W Xe lamp ($\lambda > 420$ nm)	118.69 μmol·g^{-1}·h^{-1} (CO)	97.25	[76]
CTFB$_{10}$	/	TEA	300 W Xe lamp ($\lambda > 420$ nm)	27.4 μmol·L^{-1} (CH_4)	90.3	[77]
Br-COFs@BiOCl	/	/	300 W Xe lamp ($\lambda > 320$ nm)	27.4 μmol·g^{-1}·h^{-1} (CO)	≈100	[78]
CTF/$Bi_{19}S_{27}Br_3$	/	/	AM 1.5 G	572.2 μmol·g^{-1}·h^{-1} (CO)	99.9	[79]
Fe-COF	/	/	300 W Xe lamp ($320 < \lambda < 780$ nm)	992 μmol·g^{-1}·h^{-1} (CO)	≈100	[80]
SCTF/$ZnIn_2S_4$	/	FFA	AM 1.5 G	207.8 μmol·g^{-1}·h^{-1} (CO)	≈100	[81]
DA-CTF@DPT-Co	/	TEOA	300 W Xe lamp ($\lambda > 420$ nm)	724 μmol·g^{-1}·h^{-1} (CO) 695 μmol·g^{-1}·h^{-1} (H_2)	/	[82]
Ni-PT-CTF	/	TEOA	300 W Xe lamp ($\lambda > 420$ nm)	784.5 μmol·g^{-1}·h^{-1} (CO)	96.6	[83]
TPy-COF-Co	[Ru(bpy)$_3$]Cl_2	TEOA	300 W Xe lamp ($\lambda > 420$ nm)	426,000 μmol·g^{-1}·h^{-1} (CO) 343,000 μmol·g^{-1}·h^{-1} (H_2)	/	[84]
Cu_2O/SnO_2/CTF	/	AA	250 W high pressure Hg discharge lamp	40.33 μmol·g^{-1}·h^{-1} (CO)	≈100	[85]

Li et al. [81] fabricated spherical SCTF cores by reacting cyanuric chloride and thiocyanuric acid, then coating these cores with $ZnIn_2S_4$ nanosheets using a low-temperature hydrothermal process, resulting in a core–shell SCTF/$ZnIn_2S_4$-x structure (Figure 10a). SEM and TEM images reveal that SCTF has a spherical shape with a diameter of around 1 μm, while $ZnIn_2S_4$ tends to form aggregates. In the composite, SCTF serves as a substrate for the growth of $ZnIn_2S_4$, with the $ZnIn_2S_4$ nanosheets forming a layer on the SCTF surface (Figure 9b–d). This composite material creates an S-scheme heterojunction due to its well-matched band structure. When exposed to light, electrons accumulate in the SCTF core, and holes accumulate at the $ZnIn_2S_4$ shell, with each component participating in CO_2 reduction and furfuryl alcohol oxidation, respectively (Figure 10e). The photocatalytic activity of the composite material was evaluated under simulated sunlight (AM 1.5G filter). As shown in the star diagram, the composite significantly outperformed both SCTF and $ZnIn_2S_4$ in various aspects of the photocatalytic reaction (Figure 10f). The results demonstrate that the composite material achieved a CO yield of 263.5 $\mu mol \cdot g^{-1}$ over a 6 h period in CO_2 reduction, which was substantially higher than the yields from the individual SCTF (37.1 $\mu mol \cdot g^{-1}$) and $ZnIn_2S_4$ (49.6 $\mu mol \cdot g^{-1}$) (Figure 10g). Moreover, the composite material showed a 95% conversion rate and nearly 100% selectivity in the oxidation of furfuryl alcohol to furfural (Figure 9h,i). Further analysis of reaction intermediates, pathways, and adsorption energies in both CO_2 reduction and furfuryl alcohol oxidation reactions led to the development of a comprehensive mechanism, as depicted in Figure 10j.

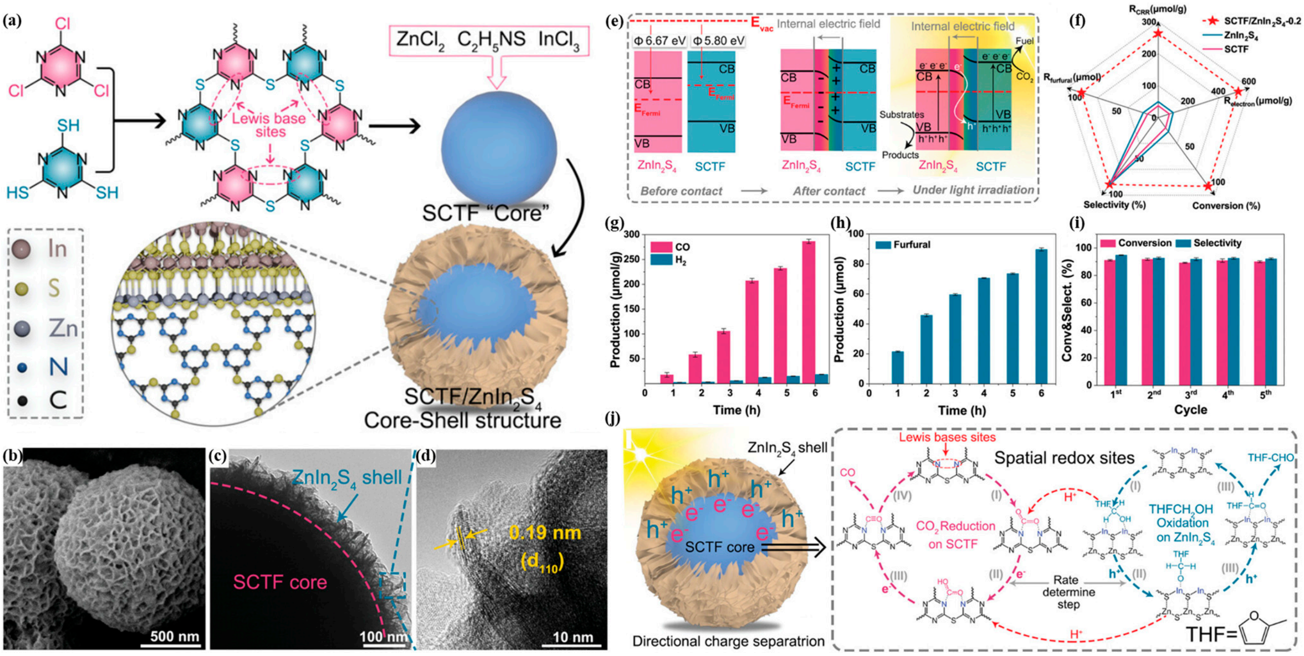

Figure 10. (**a**) Illustration of the preparation process for the SCTF/$ZnIn_2S_4$ core–shell photocatalysts. (**b**) SEM image of SCTF/$ZnIn_2S_4$-0.2 composite. (**c**,**d**) TEM images showcasing the SCTF/$ZnIn_2S_4$-0.2 structure. (**e**) Diagram illustrating the electron transfer mechanism between SCTF and $ZnIn_2S_4$. (**f**) Radar charts comparing the catalytic activity. (**g**) CO and H_2 production rates from photocatalytic CO_2 reduction using SCTF/$ZnIn_2S_4$-0.2. (**h**) Production of furfural via photocatalytic oxidation of furfuryl alcohol using SCTF/$ZnIn_2S_4$-0.2. (**i**) Stability analysis of SCTF/$ZnIn_2S_4$-0.2 during photocatalytic furfuryl alcohol oxidation. (**j**) Depiction of the photocatalytic CO_2 reduction and furfuryl alcohol oxidation mechanisms on SCTF/$ZnIn_2S_4$. Reproduced with the permission of ref. [81]. Copyright 2024, Wiley-VCH.

3.4. Other Photocatalytic Reactions

Researchers have also explored the use of CTF-based composite materials in additional photocatalytic processes, such as the oxygen evolution reaction (OER) [86–89] and pollutant degradation [90–95].

The OER, a key half-reaction in water splitting, is more complex than the hydrogen evolution reaction, as it simultaneously transfers four electrons, breaks O-H bonds, and forms O-O bonds. Given the excellent performance of ruthenium catalysts in water oxidation reactions and their extensive research, Salati et al. [86] proposed the combination of Ru-tda water oxidation catalysts with CTFs to form a binary composite material for photocatalytic oxygen production. The photoluminescence and time-resolved photoluminescence measurements showed that a pure CTF had weak electron transfer properties, whether or not electron acceptors were added (Figure 11a). In contrast, the Ru-CTF composite significantly reduced carrier recombination, with PL decay occurring faster than the instrument's response time in the TRPL tests (Figure 11b). Photocatalytic OER tests were performed in a buffered aqueous solution with a pH of 7 with sacrificial agent added. The results revealed that the composite efficiently catalyzed water oxidation (Figure 11c), achieving maximum turnover frequencies of 17 h^{-1} and turnover numbers around 220. It surpassed most of the currently reported CTF-based water oxidation catalysts in activity.

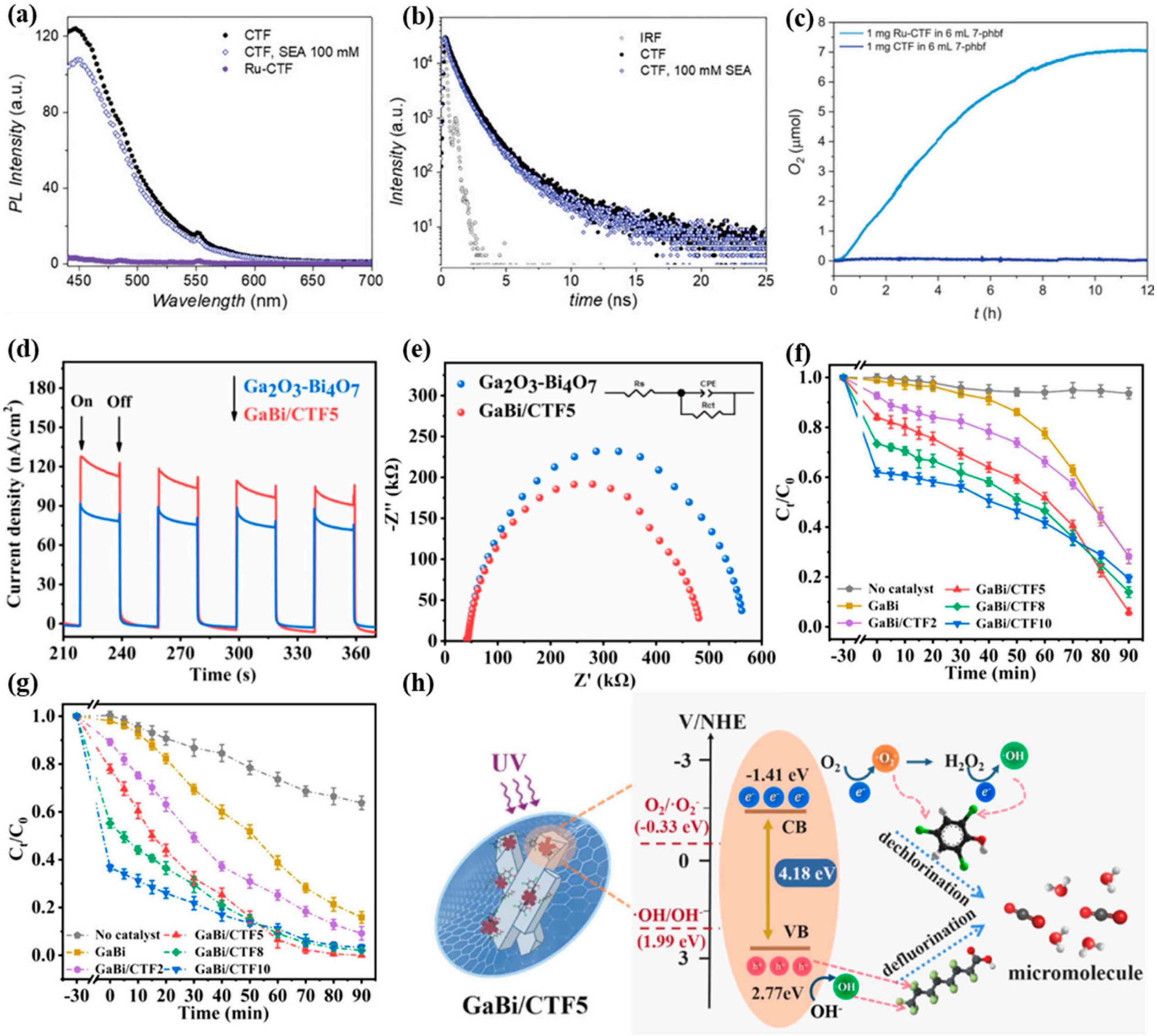

Figure 11. (**a**) PL spectra and (**b**) TRPL spectra for various samples (CTF, CTF with sacrificial agent, and Ru-CTF). (**c**) Evaluation of photocatalytic oxygen generation for the CTF and Ru-CTF. Reproduced with the permission of ref. [86]. Copyright 2024, Wiley-VCH. (**d**) Transient photocurrent measurements and (**e**) EIS results for Ga_2O_3-Bi_4O_7 and the GaBi/CTF composite. Photocatalytic degradation graphs for (**f**) perfluorooctanoic acid and (**g**) 2,4,6-trichlorophenol in mixed solutions of different samples (GaBi and GaBi/CTFx) under UV light exposure. (**h**) Photocatalytic degradation mechanism of GaBi/CTF composite on perfluorooctanoic acid and 2,4,6-trichlorophenol mixtures. Reproduced with the permission of ref. [94]. Copyright 2024, Elsevier.

Wang et al. [94] focused on two key pollutants in wastewater, perfluorooctanoic acid and 2,4,6-trichlorophenol, by combining Ga_2O_3-Bi_4O_7 heterojunctions with a fluorinated CTF (F-CTF). The addition of F-CTF created numerous micropores, significantly improving the composite's adsorption capacity. Electrochemical tests revealed that the excellent electron transport efficiency of F-CTF enhanced charge separation in the composite (Figure 11d,e). The composite's ability to degrade mixed pollutants perfluorooctanoic acid and 2,4,6-trichlorophenol was then investigated, as shown in Figure 11f,g. The results demonstrated that GaBi/CTF5 (with 5% CTF by mass) achieved the highest activity, successfully degrading 93% of perfluorooctanoic acid and 100% of 2,4,6-trichlorophenol in just 90 min. Further experiments, including quenching and electron spin resonance, helped identify the reactive species involved in the degradation process, ultimately revealing the reaction mechanism shown in Figure 11h. The composite, with a conduction band potential of -1.41 eV (lower than -0.33 eV, which is the redox potential of $O_2/{\cdot}O_2{}^{-}$), can reduce O_2 to generate ${\cdot}O_2{}^{-}$, which then produces ·OH. Meanwhile, the oxidation of pollutants is mediated by the holes present in the valence band.

4. Conclusions and Outlook

CTFs, porous organic polymers, offer distinct advantages in photocatalysis, owing to their triazine structure, stable π-conjugated system, large surface area, and excellent chemical stability. However, their standalone performance has limitations, making it necessary to combine CTFs with other materials to enhance their photocatalytic activity. This review outlines several methods for developing CTF-based composites and discusses their recent applications in photocatalysis. The progress in CTF-based composite materials is advancing quickly, and this paper provides a glimpse into future research directions in this area.

4.1. Superior Composite Materials

For further advancement in this field, it is essential to develop catalysts with enhanced performance. According to the requirements of photocatalytic reactions, optimization can be carried out from perspectives such as the light absorption range, charge carrier separation efficiency, and band structure, in order to design superior CTF-based composite materials.

4.2. Deeper Understanding of Reaction Mechanisms

Currently, research on the reaction mechanisms of CTF-based composite materials in photocatalysis remains insufficient, which is largely related to the complexity of the materials themselves. Various in situ characterization techniques, such as in situ XPS and in situ infrared spectroscopy, have been developed, greatly facilitating our understanding of the reaction process. Additionally, theoretical calculations can simulate the reaction process from a non-experimental perspective. The integration of multiple techniques helps to enhance our understanding of the reaction mechanisms of composite materials, thereby contributing to the development of more efficient catalysts.

4.3. Large-Scale Applications

At present, the application of CTF-based composite materials in the field of photocatalysis remains confined to laboratory stages and has not been implemented in large-scale industrial applications. The underlying reasons may involve the synthesis cost of the materials. However, for the development of this field, practicality is a crucial issue that must be addressed. Therefore, current research on CTF-based composite materials should take into account economic feasibility, aiming for large-scale application.

In conclusion, the research on CTF-based composite materials in the field of photocatalysis still holds significant potential, and it requires researchers to invest more time and effort. Based on the existing foundation, gradual improvements in this area of research are expected, and it is believed that more options will be provided for solar energy utilization in the future.

Author Contributions: Y.W. and Q.Z. conducted the information search and wrote the first draft of the manuscript, and X.W., Y.L., J.M., Y.H., L.G. and W.D. discussed and revised parts of the manuscript. All authors have read and agreed to the published version of the manuscript.

Funding: This research was funded by the National Key Research and Development Program of China (2021YFA1501404), Natural Science Foundation of Shanghai (22ZR1404200), and the Science and Technology Commission of Shanghai Municipality (2024ZDSYS02).

Conflicts of Interest: The authors declare no conflicts of interest.

References

1. Chen, J.; Xie, Q.; Shahbaz, M.; Song, M.; Wu, Y. The Fossil Energy Trade Relations Among BRICS Countries. *Energy* **2021**, *217*, 119383. [CrossRef]
2. Fujishima, A.; Honda, K. Electrochemical Photolysis of Water at a Semiconductor Electrode. *Nature* **1972**, *238*, 37–38. [CrossRef] [PubMed]
3. Zhu, C.; Wang, X. Nanomaterial ZnO Synthesis and Its Photocatalytic Applications: A Review. *Nanomaterials* **2025**, *15*, 682. [CrossRef] [PubMed]
4. Cheng, L.; Xiang, Q.; Liao, Y.; Zhang, H. CdS-Based Photocatalysts. *Energy Environ. Sci.* **2018**, *11*, 1362–1391. [CrossRef]
5. Wang, S.; Li, C.; Qi, Y.; Zhang, J.; Wang, N.; Liu, M.; Zhang, B.; Cai, X.; Zhang, H.; Wei, S.-H.; et al. Etched $BiVO_4$ Photocatalyst with Charge Separation Efficiency Exceeding 90%. *Nat. Commun.* **2025**, *16*, 3776. [CrossRef]
6. Ding, Y.; Wang, C.; Pei, L.; Maitra, S.; Mao, Q.; Zheng, R.; Liu, M.; Ng, Y.H.; Zhong, J.; Chen, L.-H.; et al. Emerging Heterostructured C_3N_4 Photocatalysts for Photocatalytic Environmental Pollutant Elimination and Sterilization. *Inorg. Chem. Front.* **2023**, *10*, 3756–3780. [CrossRef]
7. Spies, L.; Carmo, M.E.G.; Döblinger, M.; Xu, Z.; Xue, T.; Hartschuh, A.; Bein, T.; Schneider, J.; Patrocinio, A.O.T. Designing Atomically Precise and Robust COF Hybrids for Efficient Photocatalytic CO_2 Reduction. *Small* **2025**, *21*, 2500550. [CrossRef]
8. Doan, T.D.; Vu, N.-N.; Hoang, T.L.G.; Nguyen-Tri, P. Metal-Organic Framework (MOF)-Based Materials for Photocatalytic Antibacterial Applications. *Coord. Chem. Rev.* **2025**, *523*, 216298. [CrossRef]
9. Liu, M.; Huang, Q.; Wang, S.; Li, Z.; Li, B.; Jin, S.; Tan, B. Crystalline Covalent Triazine Frameworks by In Situ Oxidation of Alcohols to Aldehyde Monomers. *Angew. Chem. Int. Ed.* **2018**, *57*, 11968–11972. [CrossRef]
10. Gao, Z.; Jian, Y.; Yang, S.; Xie, Q.; Ross Mcfadzean, C.J.; Wei, B.; Tang, J.; Yuan, J.; Pan, C.; Yu, G. Interfacial Ti−S Bond Modulated S-Scheme MOF/Covalent Triazine Framework Nanosheet Heterojunctions for Photocatalytic C−H Functionalization. *Angew. Chem. Int. Ed.* **2023**, *62*, e202304173. [CrossRef]
11. Kuhn, P.; Antonietti, M.; Thomas, A. Porous, Covalent Triazine-Based Frameworks Prepared by Ionothermal Synthesis. *Angew. Chem. Int. Ed.* **2008**, *47*, 3450–3453. [CrossRef] [PubMed]
12. Katekomol, P.; Roeser, J.; Bojdys, M.; Weber, J.; Thomas, A. Covalent Triazine Frameworks Prepared from 1,3,5-Tricyanobenzene. *Chem. Mater.* **2013**, *25*, 1542–1548. [CrossRef]
13. Yu, S.-Y.; Mahmood, J.; Noh, H.-J.; Seo, J.-M.; Jung, S.-M.; Shin, S.-H.; Im, Y.-K.; Jeon, I.-Y.; Baek, J.-B. Direct Synthesis of a Covalent Triazine-Based Framework from Aromatic Amides. *Angew. Chem. Int. Ed.* **2018**, *57*, 8438–8442. [CrossRef] [PubMed]
14. Ren, S.; Bojdys, M.J.; Dawson, R.; Laybourn, A.; Khimyak, Y.Z.; Adams, D.J.; Cooper, A.I. Porous, Fluorescent, Covalent Triazine-Based Frameworks via Room-Temperature and Microwave-Assisted Synthesis. *Adv. Mater.* **2012**, *24*, 2357–2361. [CrossRef]
15. Wang, K.; Yang, L.-M.; Wang, X.; Guo, L.; Cheng, G.; Zhang, C.; Jin, S.; Tan, B.; Cooper, A. Covalent Triazine Frameworks via a Low-Temperature Polycondensation Approach. *Angew. Chem. Int. Ed.* **2017**, *56*, 14149–14153. [CrossRef]
16. Xiang, Z.; Cao, D. Synthesis of Luminescent Covalent–Organic Polymers for Detecting Nitroaromatic Explosives and Small Organic Molecules. *Macromol. Rapid Commun.* **2012**, *33*, 1184–1190. [CrossRef]
17. Meier, C.B.; Sprick, R.S.; Monti, A.; Guiglion, P.; Lee, J.-S.M.; Zwijnenburg, M.A.; Cooper, A.I. Structure-property Relationships for Covalent Triazine-Based Frameworks: The Effect of Spacer Length on Photocatalytic Hydrogen Evolution from Water. *Polymer* **2017**, *126*, 283–290. [CrossRef]
18. Zhao, W.; Ding, J.; Zou, Y.; Di, C.-a.; Zhu, D. Chemical Doping of Organic Semiconductors for Thermoelectric Applications. *Chem. Soc. Rev.* **2020**, *49*, 7210–7228. [CrossRef]
19. Lüssem, B.; Riede, M.; Leo, K. Doping of Organic Semiconductors. *Phys. Status Solidi (A)* **2013**, *210*, 9–43. [CrossRef]

20. Cheng, Z.; Zheng, K.; Lin, G.; Fang, S.; Li, L.; Bi, J.; Shen, J.; Wu, L. Constructing a Novel Family of Halogen-Doped Covalent Triazine-Based Frameworks as Efficient Metal-Free Photocatalysts for Hydrogen Production. *Nanoscale Adv.* **2019**, *1*, 2674–2680. [CrossRef]
21. Li, S.; Wu, M.-F.; Guo, T.; Zheng, L.-L.; Wang, D.; Mu, Y.; Xing, Q.-J.; Zou, J.-P. Chlorine-mediated Photocatalytic Hydrogen Production Based on Triazine Covalent Organic Framework. *Appl. Catal. B Environ.* **2020**, *272*, 118989. [CrossRef]
22. Niu, Q.; Cheng, Z.; Chen, Q.; Huang, G.; Lin, J.; Bi, J.; Wu, L. Constructing Nitrogen Self-Doped Covalent Triazine-Based Frameworks for Visible-Light-Driven Photocatalytic Conversion of CO_2 into CH_4. *ACS Sustain. Chem. Eng.* **2021**, *9*, 1333–1340. [CrossRef]
23. Han, X.; Zhao, F.; Shang, Q.; Zhao, J.; Zhong, X.; Zhang, J. Effect of Nitrogen Atom Introduction on the Photocatalytic Hydrogen Evolution Activity of Covalent Triazine Frameworks: Experimental and Theoretical Study. *ChemSusChem* **2022**, *15*, e202200828. [CrossRef] [PubMed]
24. Cheng, Z.; Fang, W.; Zhao, T.; Fang, S.; Bi, J.; Liang, S.; Li, L.; Yu, Y.; Wu, L. Efficient Visible-Light-Driven Photocatalytic Hydrogen Evolution on Phosphorus-Doped Covalent Triazine-Based Frameworks. *ACS Appl. Mater. Interfaces* **2018**, *10*, 41415–41421. [CrossRef]
25. Li, L.; Fang, W.; Zhang, P.; Bi, J.; He, Y.; Wang, J.; Su, W. Sulfur-doped Covalent Triazine-Based Frameworks for Enhanced Photocatalytic Hydrogen Evolution from Water Under Visible Light. *J. Mater. Chem. A* **2016**, *4*, 12402–12406. [CrossRef]
26. Zhu, C.; Fang, Q.; Liu, R.; Dong, W.; Song, S.; Shen, Y. Insights into the Crucial Role of Electron and Spin Structures in Heteroatom-Doped Covalent Triazine Frameworks for Removing Organic Micropollutants. *Environ. Sci. Technol.* **2022**, *56*, 6699–6709. [CrossRef]
27. He, J.; Wang, X.; Jin, S.; Liu, Z.-Q.; Zhu, M. 2D Metal-Free Heterostructure of Covalent Triazine Framework/g-C_3N_4 for Enhanced Photocatalytic CO_2 Reduction with High Selectivity. *Chin. J. Catal.* **2022**, *43*, 1306–1315. [CrossRef]
28. Zhang, L.; Zhang, Y.; Huang, X.; Tao, L.; Bi, Y. Direct Observation of Dynamic Interfacial Bonding and Charge Transfer in Metal-Free Photocatalysts for Efficient Hydrogen Evolution. *Appl. Catal. B Environ.* **2021**, *283*, 119633. [CrossRef]
29. Lim, S.Y.; Shen, W.; Gao, Z. Carbon Quantum Dots and Their Applications. *Chem. Soc. Rev.* **2015**, *44*, 362–381. [CrossRef]
30. Yang, Y.; Guo, Q.; Li, Q.; Guo, L.; Chu, H.; Liao, L.; Wang, X.; Li, Z.; Zhou, W. Carbon Quantum Dots Confined into Covalent Triazine Frameworks for Efficient Overall Photocatalytic H_2O_2 Production. *Adv. Funct. Mater.* **2024**, *34*, 2400612. [CrossRef]
31. Chen, M.; Sun, Z.; Wei, T.; Zhang, B.; Guo, K.; Feng, Y.; Zhang, B. Highly Crystalline Covalent Triazine Framework@rGO Hybrids with Ultra-High Stacking Stability for Efficient Photocatalytic CO_2 Fixation. *Chem. Eng. J.* **2025**, *508*, 160982. [CrossRef]
32. He, Y.; Chen, X.; Huang, C.; Li, L.; Yang, C.; Yu, Y. Encapsulation of Co Single Sites in Covalent Triazine Frameworks for Photocatalytic Production of Syngas. *Chin. J. Catal.* **2021**, *42*, 123–130. [CrossRef]
33. Ran, L.; Li, Z.; Ran, B.; Cao, J.; Zhao, Y.; Shao, T.; Song, Y.; Leung, M.K.H.; Sun, L.; Hou, J. Engineering Single-Atom Active Sites on Covalent Organic Frameworks for Boosting CO_2 Photoreduction. *J. Am. Chem. Soc.* **2022**, *144*, 17097–17109. [CrossRef]
34. Huang, G.; Niu, Q.; He, Y.; Tian, J.; Gao, M.; Li, C.; An, N.; Bi, J.; Zhang, J. Spatial Confinement of Copper Single Atoms into Covalent Triazine-Based Frameworks for Highly Efficient and Selective Photocatalytic CO_2 Reduction. *Nano Res.* **2022**, *15*, 8001–8009. [CrossRef]
35. Li, J.; Liu, P.; Tang, Y.; Huang, H.; Cui, H.; Mei, D.; Zhong, C. Single-Atom Pt–N_3 Sites on the Stable Covalent Triazine Framework Nanosheets for Photocatalytic N_2 Fixation. *ACS Catal.* **2020**, *10*, 2431–2442. [CrossRef]
36. Gao, S.; Zhang, P.; Huang, G.; Chen, Q.; Bi, J.; Wu, L. Band Gap Tuning of Covalent Triazine-Based Frameworks through Iron Doping for Visible-Light-Driven Photocatalytic Hydrogen Evolution. *ChemSusChem* **2021**, *14*, 3850–3857. [CrossRef]
37. Li, Z.; Qiu, S.; Song, Y.; Huang, S.; Gao, J.; Sun, L.; Hou, J. Engineering Single–Atom Active Sites Anchored Covalent Organic Frameworks for Efficient Metallaphotoredox CN Cross–coupling Reactions. *Sci. Bull.* **2022**, *67*, 1971–1981. [CrossRef]
38. Xu, Z.; Cui, Y.; Guo, B.; Li, H.-Y.; Li, H.-X. Boosting Visible-Light-Driven H_2 Evolution of Covalent Triazine Framework from Water by Modifying Ni(II) Pyrimidine-2-thiolate Cocatalyst. *ChemCatChem* **2021**, *13*, 958–965. [CrossRef]
39. Bulushev, D.A.; Golub, F.S.; Trubina, S.V.; Zvereva, V.V.; Bulusheva, L.G.; Gerasimov, E.Y.; Navlani-García, M.; Krot, A.D.; Jena, H.S. Single-Atom Pd Catalysts Supported on Covalent Triazine Frameworks for Hydrogen Production from Formic Acid. *ACS Appl. Nano Mater.* **2022**, *5*, 12887–12896. [CrossRef]
40. Xu, N.; Diao, Y.; Xu, Z.; Ke, H.; Zhu, X. Covalent Triazine Frameworks Embedded with Ir Complexes for Enhanced Photocatalytic Hydrogen Evolution. *ACS Appl. Energy Mater.* **2022**, *5*, 7473–7478. [CrossRef]
41. Xiong, Y.; Qin, Y.; Su, L.; Ye, F. Bioinspired Synthesis of Cu^{2+}-Modified Covalent Triazine Framework: A New Highly Efficient and Promising Peroxidase Mimic. *Chem. A Eur. J.* **2017**, *23*, 11037–11045. [CrossRef] [PubMed]
42. Chen, J.; Li, G.; Lu, N.; Lin, H.; Zhou, S.; Liu, F. Anchoring Cobalt Single Atoms on 2D Covalent Triazine Framework with Charge Nanospatial Separation for Enhanced Photocatalytic Pollution Degradation. *Mater. Today Chem.* **2022**, *24*, 100832. [CrossRef]
43. Zhu, C.; Lu, L.; Fang, Q.; Song, S.; Chen, B.; Shen, Y. Unveiling Spin State-Dependent Micropollutant Removal using Single-Atom Covalent Triazine Framework. *Adv. Funct. Mater.* **2023**, *33*, 2210905. [CrossRef]

44. Zhu, C.; Yao, Y.; Fang, Q.; Song, S.; Chen, B.; Shen, Y. Unveiling the Dynamic Evolution of Single-Atom Co Sites in Covalent Triazine Frameworks for Enhanced H_2O_2 Photosynthesis. *ACS Catal.* **2024**, *14*, 2847–2858. [CrossRef]
45. Liu, S.; Zhu, C.; Xu, J.; Lu, L.; Fang, Q.; Xu, C.; Zheng, Y.; Song, S.; Shen, Y. Efficient Dual-pathway H_2O_2 Production Promoted by Covalent Triazine Frameworks with Integrated Dual Active Sites. *Appl. Catal. B Environ. Energy* **2024**, *344*, 123629. [CrossRef]
46. Han, X.; Dong, Y.; Zhao, J.; Ming, S.; Xie, Y. Construction of Ternary Z-scheme Covalent Triazine Framework@Au@TiO_2 for Enhanced Visible-Light-Driven Hydrogen Evolution activity. *Int. J. Hydrog. Energy* **2022**, *47*, 18334–18346. [CrossRef]
47. Xu, Z.; Cui, Y.; Young, D.J.; Wang, J.; Li, H.-Y.; Bian, G.-Q.; Li, H.-X. Combination of Co^{2+}-Immobilized Covalent Triazine Framework and TiO_2 by Covalent Bonds to Enhance Photoreduction of CO_2 to CO with H_2O. *J. CO2 Util.* **2021**, *49*, 101561. [CrossRef]
48. Chao, X.; Xu, Y.; Chen, H.; Feng, D.; Hu, J.; Yu, Y. TiO_2-Based Photocatalyst Modified with a Covalent Triazine-Based Framework Organocatalyst for Carbamazepine Photodegradation. *RSC Adv.* **2021**, *11*, 6943–6951. [CrossRef]
49. Oyegbeda, O.; Akpotu, S.O.; Moodley, B. Dual Functional Covalent Triazine Framework-TiO_2 S-scheme Heterojunction for Efficient Sequestration of Ciprofloxacin: Mechanism and Degradation Products. *Environ. Res.* **2025**, *266*, 120501. [CrossRef]
50. Li, J.; Xia, Y.; Zhang, Z.; Zhao, X.; Wang, L.; Huang, J.; She, H.; Li, X.; Wang, Q. Regulating the Layer Stacking Configuration of CTF-TiO_2 Heterostructure for Improving the Photocatalytic CO_2 Reduction. *Inorg. Chem.* **2024**, *63*, 19344–19354. [CrossRef]
51. Xia, B.; Liu, G.; Fan, K.; Chen, R.; Liu, X.; Li, L. Boosting Hydrogen Peroxide Photosynthesis via a 1D/2D S-scheme Heterojunction Constructed by a Covalent Triazine Framework with Dual O_2 Reduction Centers. *Chin. J. Catal.* **2025**, *69*, 315–326. [CrossRef]
52. Sayed, M.; Xu, F.; Kuang, P.; Low, J.; Wang, S.; Zhang, L.; Yu, J. Sustained CO_2-Photoreduction Activity and High Selectivity over Mn, C-Codoped ZnO Core-Triple Shell Hollow Spheres. *Nat. Commun.* **2021**, *12*, 4936. [CrossRef] [PubMed]
53. Jiang, Z.; Cheng, B.; Zhang, L.; Zhang, Z.; Bie, C. A Review on ZnO-based S-scheme Heterojunction Photocatalysts. *Chin. J. Catal.* **2023**, *52*, 32–49. [CrossRef]
54. Wang, D.; Zeng, H.; Xiong, X.; Wu, M.-F.; Xia, M.; Xie, M.; Zou, J.-P.; Luo, S.-L. Highly Efficient Charge Transfer in CdS-Covalent Organic Framework Nanocomposites for Stable Photocatalytic Hydrogen Evolution under Visible Light. *Sci. Bull.* **2020**, *65*, 113–122. [CrossRef] [PubMed]
55. Guo, S.; Yang, P.; Zhao, Y.; Yu, X.; Wu, Y.; Zhang, H.; Yu, B.; Han, B.; George, M.W.; Liu, Z. Direct Z-Scheme Heterojunction of SnS_2/Sulfur-Bridged Covalent Triazine Frameworks for Visible-Light-Driven CO_2 Photoreduction. *ChemSusChem* **2020**, *13*, 6278–6283. [CrossRef]
56. Yang, X.; Bai, X.; Ma, Y.; He, D.; Wang, X.; Guo, Y. A Solar Light Regenerated Adsorbent by Implanting CdS into An Active Covalent Triazine Framework to Decontaminate Tetracycline. *Sep. Purif. Technol.* **2021**, *255*, 117696. [CrossRef]
57. Jiang, Q.; Sun, L.; Bi, J.; Liang, S.; Li, L.; Yu, Y.; Wu, L. MoS2 Quantum Dots-Modified Covalent Triazine-Based Frameworks for Enhanced Photocatalytic Hydrogen Evolution. *ChemSusChem* **2018**, *11*, 1108–1113. [CrossRef]
58. Huang, H.; Xu, B.; Tan, Z.; Jiang, Q.; Fang, S.; Li, L.; Bi, J.; Wu, L. A Facile In Situ Growth of CdS Quantum Dots on Covalent Triazine-Based Frameworks for Photocatalytic H_2 Production. *J. Alloys Compd.* **2020**, *833*, 155057. [CrossRef]
59. Zhang, G.; Li, X.; Chen, D.; Li, N.; Xu, Q.; Li, H.; Lu, J. Internal Electric Field and Adsorption Effect Synergistically Boost Carbon Dioxide Conversion on Cadmium Sulfide@Covalent Triazine Frameworks Core–Shell Photocatalyst. *Adv. Funct. Mater.* **2023**, *33*, 2308553. [CrossRef]
60. Zhou, T.; Han, X.; Shen, W.; Ji, F.; Liu, M.; Song, Y.; He, W.-W. Construction of NiS/CTF Heterojunction Photocatalyst with An Outstanding Photocatalytic Hydrogen Evolution Performance. *Chin. Chem. Lett.* **2024**, 110415. [CrossRef]
61. Mishra, A.; Mehta, A.; Basu, S.; Shetti, N.P.; Reddy, K.R.; Aminabhavi, T.M. Graphitic Carbon Nitride (g–C_3N_4)–Based Metal-Free Photocatalysts for Water Splitting: A Review. *Carbon* **2019**, *149*, 693–721. [CrossRef]
62. Yang, Y.; Niu, W.; Dang, L.; Mao, Y.; Wu, J.; Xu, K. Recent Progress in Doped g-C_3N_4 Photocatalyst for Solar Water Splitting: A Review. *Front. Chem.* **2022**, *10*, 955065. [CrossRef] [PubMed]
63. Zang, J.; Zhao, Y.; Yu, L.; Young, D.J.; Ren, Z.-G.; Li, H.-X. Covalent Organic Framework Spherical Nanofibers Bearing Carbon Quantum Dots for Boosting Photocatalytic Hydrogen Production. *J. Mater. Chem. A* **2025**, *13*, 1932–1941. [CrossRef]
64. Chen, L.; Chen, G.; Gong, C.; Zhang, Y.; Xing, Z.; Li, J.; Xu, G.; Li, G.; Peng, Y. Low-Valence Platinum Single Atoms in Sulfur-Containing Covalent Organic Frameworks for Photocatalytic Hydrogen Evolution. *Nat. Commun.* **2024**, *15*, 10501. [CrossRef]
65. Huang, K.; Chen, D.; Zhang, X.; Shen, R.; Zhang, P.; Xu, D.; Li, X. Constructing Covalent Triazine Frameworks/N-Doped Carbon-Coated Cu_2O S-Scheme Heterojunctions for Boosting Photocatalytic Hydrogen Production. *Acta Phys. Chim. Sin.* **2024**, *40*, 2407020. [CrossRef]
66. Sun, Q.-G.; Yang, C.-L.; Li, X.; Liu, Y.; Zhao, W.; Ma, X. Photocatalytic Overall Water Splitting Z-Schemes for Hydrogen Production with the X@CTF-0/β-Sb (X = S, Se) Heterostructures. *Colloids Surf. A Physicochem. Eng. Asp.* **2024**, *703*, 135437. [CrossRef]
67. Yao, Y.; Lin, J.; Liu, S.; Zheng, Y.; Lu, L.; Fang, Q.; Song, S.; Zhu, C.; Shen, Y. A Pyridine-Woven Covalent Organic Framework Facilitating the Immobilization of Co Single Atoms towards Efficient Photocatalytic H_2 Evolution. *J. Mater. Chem. A* **2024**, *12*, 31619–31629. [CrossRef]

68. Wang, M.; Li, Y.; Yan, D.; Hu, H.; Song, Y.; Su, X.; Sun, J.; Xiao, S.; Gao, Y. Dipole Polarization Modulating of Vinylene-Linked Covalent Organic Frameworks for Efficient Photocatalytic Hydrogen Evolution. *Chin. J. Catal.* **2024**, *65*, 103–112. [CrossRef]
69. Li, C.; Guan, L.; Zhang, J.; Cheng, C.; Guo, Z.; Tian, Z.; Yang, L.-M.; Jin, S. Regulating Pt-covalent Triazine Framework Schottky Junctions by Using Tailor-Made Nitrogen Sites towards Efficient Photocatalysis. *J. Mater. Chem. A* **2024**, *12*, 13876–13881. [CrossRef]
70. Zhang, F.; Lv, X.; Wang, H.; Cai, J.; Wang, H.; Bi, S.; Wei, R.; Yang, C.; Zheng, G.; Han, Q. p-π Conjugated Covalent Organic Frameworks Expedite Molecular Triplet Excitons for H_2O_2 Production Coupled with Biomass Upgrading. *Adv. Mater.* **2025**, *37*, 2502220. [CrossRef]
71. Liu, Y.; Li, L.; Tan, H.; Ye, N.; Gu, Y.; Zhao, S.; Zhang, S.; Luo, M.; Guo, S. Fluorination of Covalent Organic Framework Reinforcing the Confinement of Pd Nanoclusters Enhances Hydrogen Peroxide Photosynthesis. *J. Am. Chem. Soc.* **2023**, *145*, 19877–19884. [CrossRef] [PubMed]
72. Ren, W.; Li, N.; Chang, Q.; Wu, J.; Yang, J.; Hu, S.; Kang, Z. Abstracting Photogenerated Holes from Covalent Triazine Frameworks through Carbon Dots for Overall Hydrogen Peroxide Photosynthesis. *Chin. J. Catal.* **2024**, *62*, 178–189. [CrossRef]
73. Yang, L.; Lv, W.; Wang, Y.; Wang, Y. Carbon Nanotube Incorporation and Framework Protonation-Regulated Energy Band for Enhanced Photocatalytic Hydrogen Peroxide Production of COF. *Nano Res.* **2025**, *18*, 94907024. [CrossRef]
74. Wang, H.; Yang, C.; Chen, F.; Zheng, G.; Han, Q. A Crystalline Partially Fluorinated Triazine Covalent Organic Framework for Efficient Photosynthesis of Hydrogen Peroxide. *Angew. Chem. Int. Ed.* **2022**, *61*, e202202328. [CrossRef]
75. Wang, H.; Jin, S.; Zhang, X.; Xie, Y. Excitonic Effects in Polymeric Photocatalysts. *Angew. Chem. Int. Ed.* **2020**, *59*, 22828–22839. [CrossRef]
76. Wang, X.; Wang, J.; Shen, F.; Zhang, Y.; Zhang, L.; Zang, L.; Sun, L. Engineered Covalent Triazine Framework Inverse Opal Beads for Enhanced Photocatalytic Carbon Dioxide Reduction. *J. Colloid Interface Sci.* **2025**, *689*, 137244. [CrossRef]
77. Chen, S.; Huang, G.; Sheng, H.; Huang, G.; Sa, R.; Chen, Q.; Bi, J. Asymmetric Electronic Distribution Induced Enhancement in Photocatalytic CO_2-to-CH_4 Conversion via Boron-Doped Covalent Triazine Frameworks. *J. Colloid Interface Sci.* **2025**, *685*, 766–773. [CrossRef]
78. Wang, Y.; Cao, Y.; Wei, S.; Li, M.; Wang, H.; Yu, B.; Li, J.; Huang, J. N-Bi Covalently Connected Z-Scheme Heterojunction by In Situ Anchoring Biocl on Triazine-Based Bromine-Substituted Covalent Organic Frameworks for the Enhanced Photocatalytic Reduction of CO_2 and Cr (VI). *Chem. Eng. J.* **2025**, *505*, 159349. [CrossRef]
79. Zhang, J.; Zheng, M.; Wu, Y.; Xiong, J.; Li, S.; Jiang, W.; Liu, Z.; Di, J. Strongly Coupled Interface in Electrostatic Self-Assembly Covalent Triazine Framework/$Bi_{19}S_{27}Br_3$ for High-Efficiency CO_2 Photoreduction. *ACS Nano* **2025**, *19*, 2759–2768. [CrossRef]
80. Gao, S.; Zhao, X.; Zhang, Q.; Guo, L.; Li, Z.; Wang, H.; Zhang, S.; Wang, J. Mimic Metalloenzymes with Atomically Dispersed Fe Sites in Covalent Organic Framework Membranes for Enhanced CO_2 Photoreduction. *Chem. Sci.* **2025**, *16*, 1222–1232. [CrossRef]
81. Li, Q.; Li, X.; Zheng, M.; Luo, F.; Zhang, L.; Zhang, B.; Jiang, B. Spatial Coupling of Photocatalytic CO_2 Reduction and Selective Oxidation on Covalent Triazine Framework/$ZnIn_2S_4$ Core–Shell Structures. *Adv. Funct. Mater.* **2025**, *35*, 2417279. [CrossRef]
82. Kong, K.; Zhong, H.; Zhang, F.; Lv, H.; Li, X.; Wang, R. The Reduced Barrier for the Photogenerated Charge Migration on Covalent Triazine-Based Frameworks for Boosting Photocatalytic CO_2 Reduction into Syngas. *Adv. Funct. Mater.* **2025**, *35*, 2417109. [CrossRef]
83. Jiang, Y.; Xiong, L.; Guo, S.; Xu, C.; Wang, J.; Wu, X.; Xiao, Y.; Song, R. Installing Active Metal Species in a Covalent Triazine Framework for Highly Efficient and Selective Photocatalytic CO_2 Reduction. *J. Mater. Chem. A* **2024**, *12*, 32045–32053. [CrossRef]
84. Fu, P.; Chen, C.; Wu, C.; Meng, B.; Yue, Q.; Chen, T.; Yin, W.; Chi, X.; Yu, X.; Li, R.; et al. Covalent Organic Framework Stabilized Single CoN_4Cl_2 Site Boosts Photocatalytic CO_2 Reduction into Tunable Syngas. *Angew. Chem. Int. Ed.* **2025**, *64*, e202415202. [CrossRef]
85. Mandal, P.C.; Sherpa, N.D.; Sarkar, S.; Roy, C.K.; Ali, O.; Roy, N. CTF Stabilizes Truncated octahedral Cu_2O Nanocrystals and SnO_2 Nanoparticle Assisted Photocatalytic CO_2 Reduction in Hybrid Ternary Cu_2O/SnO_2/CTF Nanostructures. *CrystEngComm* **2025**, *27*, 1427–1438. [CrossRef]
86. Salati, M.; Dorchies, F.; Wang, J.-W.; Ventosa, M.; González-Carrero, S.; Bozal-Ginesta, C.; Holub, J.; Rüdiger, O.; DeBeer, S.; Gimbert-Suriñach, C.; et al. Covalent Triazine-Based Frameworks with Ru-tda Based Catalyst Anchored via Coordination Bond for Photoinduced Water Oxidation. *Small* **2025**, *21*, 2406375. [CrossRef] [PubMed]
87. Sicignano, M.; Gobbato, T.; Bonetto, R.; Centomo, P.; Di Vizio, B.; De Biasi, F.; Rosa-Gastaldo, D.; Pierantoni, C.; Bonetto, A.; Glisenti, A.; et al. Synergistic Integration of a Ru(bda)-Based Catalyst in a Covalent Organic Framework for Enhanced Photocatalytic Water Oxidation. *Adv. Sustain. Syst.* **2025**, *9*, 2400653. [CrossRef]
88. Sun, R.; Hu, X.; Shu, C.; Guo, Y.; Wang, X.; Tan, B. Covalent Triazine Frameworks with Ru Molecular Catalyst for Efficient Photocatalytic Oxygen Evolution Reaction. *Sci. China Mater.* **2024**, *67*, 642–649. [CrossRef]
89. Chen, H.; Gardner, A.M.; Lin, G.; Zhao, W.; Bahri, M.; Browning, N.D.; Sprick, R.S.; Li, X.; Xu, X.; Cooper, A.I. Covalent Triazine-Based Frameworks with Cobalt-Loading for Visible Light-Driven Photocatalytic Water Oxidation. *Catal. Sci. Technol.* **2022**, *12*, 5442–5452. [CrossRef]

90. Tang, Q.; Wan, Y.; Pan, Z.; Cheng, Q. Visible Light-Driven Triazine-Based S-scheme COF-TpTt@BiOBr Heterojunction with Oxygen Vacancy for Enhanced Photocatalytic Pollutants Removal and Hydrogen Production. *Environ. Res.* **2025**, *269*, 120901. [CrossRef]
91. Moya, A.; Sánchez-Fuente, M.; Linde, M.; Cepa-López, V.; del Hierro, I.; Díaz-Sánchez, M.; Gómez-Ruiz, S.; Mas-Ballesté, R. Enhancing Photocatalytic Performance of F-Doped TiO_2 through the Integration of Small Amounts of a Quinoline-Based Covalent Triazine Framework. *Nanoscale* **2025**, *17*, 8880–8891. [CrossRef] [PubMed]
92. Zandipak, R.; Bahramifar, N.; Younesi, H.; Zolfigol, M.A. Decoration of Carbon Nanodots on Conjugated Triazine Framework Nanosheets as Z-Scheme Heterojunction for Boosting Opto-Electro Photocatalytic Degradation of Organic Hydrocarbons from Petrochemical Wastewater. *J. Environ. Chem. Eng.* **2025**, *13*, 115380. [CrossRef]
93. Zandipak, R.; Bahramifar, N.; Younesi, H.; Zolfigol, M.A. Electro-Photocatalyst Effect of N-S-Doped Carbon Dots and Covalent Organic Triazine Framework Heterostructures for Boosting Photocatalytic Degradation of Phenanthrene in Water. *Chemosphere* **2024**, *364*, 142980. [CrossRef] [PubMed]
94. Wang, S.; Wang, S.; Tang, R.; Liu, Y.; Chen, H. Removal of Mixed Pollutants of Perfluorooctanoic Acid and 2,4,6-Trichlorophenol via Adsorption-Photocatalysis Using Ga_2O_3-Bi_4O_7 Combining with Fluorine-Doped Covalent Triazine Framework: Role of Different Active Species. *J. Colloid Interface Sci.* **2024**, *676*, 959–973. [CrossRef]
95. Qi, L.; Xiao, C.; Lu, W.; Zhang, H.; Zhou, Y.; Qi, J.; Yang, Y.; Zhu, Z.; Li, J. Triazine-based Covalent Organic Framework/g-C_3N_4 Heterojunction toward Highly Efficient Photoactivation of Peroxydisulfate for Sulfonamides Degradation. *Sep. Purif. Technol.* **2025**, *354*, 128758. [CrossRef]